SOLID-SOLUTION OF $Cd_{1-x}Zn_xS$ NANOCRYSTALS IN THE CHANNELS OF MESOSTRUCTURED SILICA FILMS

A THESIS

SUBMITTED TO THE DEPARTMENT OF CHEMISTRY

THE INSTITUTE OF ENGINEERING AND SCIENCES OF

BILKENT UNIVERSITY

IN PARTIAL FULFILLMENT OF THE REQUIREMENTS

FOR THE DEGREE

OF

MASTER OF SCIENCE

By

YAŞAR AKDOĞAN

JANUARY 2006

I certify that I have read this thesis and in my opinion it is fully adequate, in scope and quality, as a thesis of the degree of Master of Science

_____

Assoc. Prof. Dr. Ömer Dağ (Supervisor)

I certify that I have read this thesis and in my opinion it is fully adequate, in scope and quality, as a thesis of the degree of Master of Science

_____

Prof. Dr. Şefik Süzer

I certify that I have read this thesis and in my opinion it is fully adequate, in scope and quality, as a thesis of the degree of Master of Science

_____

Prof. Dr. Hüseyin İşçi

I certify that I have read this thesis and in my opinion it is fully adequate, in scope and quality, as a thesis of the degree of Master of Science

_____

Assoc. Prof. Dr. Margarita Kantcheva

I certify that I have read this this thesis and in my opinion it is fully adequate, in scope and quality, as a thesis of the degree of Master of Science

_____

Asst. Prof. Dr. Dönüş Tuncel

Approved for the Institute of Engineering and Sciences

_____

Prof. Dr. Mehmet Baray
Director of Institute of Engineering and Sciences

ABSTRACT

SOLID-SOLUTION OF $Cd_{1-x}Zn_xS$ NANOCRYSTALS IN THE CHANNELS OF MESOSTRUCTURED SILICA

YAŞAR AKDOĞAN

M.S. in Chemistry
Supervisor: Assoc. Prof. Dr. Ömer DAĞ
JANUARY 2006

Mesostructured silica can be used as a reaction medium to produce solid-solution of $Cd_{1-x}Zn_xS$ nanocrystals as thin films. These films were synthesized from oligo(ethylene oxide) non-ionic surfactant ($CH_3(CH_2)_{11}(OCH_2CH_2)_{10}OH$, ($C_{12}EO_{10}$)), cadmium and zinc nitrate salts ($[Cd(H_2O)_4](NO_3)_2$ and $[Zn(H_2O)_6](NO_3)_2$), water, and tetramethylorthosilicate (TMOS, as silica source) mixtures using a liquid crystalline templating (LCT) approach and metal containing liquid crystalline (MLC) mesophase. Metal ion to surfactant mole ratio was 1.0 which determines the stability and structure of the mesostructured silica. The mesostructured silica film has a 3D hexagonal structure with oriented channels. The silica pore size can be controlled by controlling ageing temperature and time. The pore diameter of the silica channels that aged at room temperature (RT) for two days is 4.7 nm and the one aged at 250^0 C for 30 minutes is 3.3 nm.

Cd(II) and Zn(II) incorporated film samples can be reacted at RT under H_2S atmosphere to produce zinc blend, $Cd_{1-x}Zn_xS$ nanocrystals (nano-$Cd_{1-x}Zn_xS$-meso-

SiO_2) in the channels of the mesostructured silica. The band gaps of the nano-$Cd_{1-x}Zn_xS$-meso-SiO_2 vary between 2.6 eV for CdS and 4.1 eV for ZnS. The Cd (II) rich nanoparticles are larger (4.4 nm) than Zn (II) rich nanoparticles (3.1 nm). The silica wall thickness that can be controlled by ageing at different temperatures confines the growth of the $Cd_{1-x}Zn_xS$ nanocrystals in the pores. By controlling the size of the silica channel between 4.7 and 3.3 nm, one can control the band-gap of the CdS nanocrystals between 2.6 and 2.8 eV.

Keywords: Mesostructured silica, non-ionic surfactant, mesopores, ageing, Metal containing Liquid Crystals, solid solution of $Cd_{1-x}Zn_xS$, nanoparticle, semiconductor, band-gap.

ÖZET

MEZO YAPILI SİLİKA FİLM İÇERİSİNDE $Cd_{1-x}Zn_xS$

NANOKRİSTALLERİNİN KATI ÇÖZELTİLERİ

YAŞAR AKDOĞAN

Kimya Bölümü Yüksek Lisans Tezi
Tez Yöneticisi: Doç. Dr. Ömer DAĞ
OCAK 2006

Mezoyapılı silika, $Cd_{1-x}Zn_xS$ katı çözeltilerini ince filmler halinde hazırlanmasında tepkime ortamı olarak kullanılır. İnce film numuneler oligo etilen oksit, iyonik olmayan yüzey aktif, ($CH_3(CH_2)_{11}(OCH_2CH_2)_{10}OH$, ($C_{12}EO_{10}$)), kadmiyum ve çinko nitrat tuzları ($[Cd(H_2O)_4](NO_3)_2$ ve $[Zn(H_2O)_6](NO_3)_2$), su ve tetrametilenortosilikat (TMOS, silika kaynağı) karışımından ve sıvı kristal kalıplama (SKK) yaklaşımı ve metal içeren sıvı kristal (MSK) mesofazların beraber kullanılmasıyla oluşur. Kullanılan tuz:yüzeyaktif mol oranı 1.0, ve bu oran silika mesoyapının kararlılığını ve yapısını tayin eder.Silika mezoyapı 3B hekzagonal yapıda ve oldukça düzenlidir. Silika gözenek boyutları, tepkime süresi ve sıcaklığı ile kontrol edilebilir. Oda sıcaklığında iki gün bekletilmiş filmlerde gözenek çapı 4.7 nm iken 250^0C de yarım saat bekletilmiş filmlerin gözenek çapı 3.3 nm dir.

Cd(II), Zn(II) içeren filmler hidrojen sülfür (H_2S) ile tepkimeleri sonucunda, çinko blend yapısında $Cd_{1-x}Zn_xS$ kristalleri mezoyapılı silika kanalları içerisinde oluşur. $Cd_{1-x}Zn_xS$ nanotaneciklerinin band aralıkları (E_g) 2.6 eV (CdS) ve 4.1 eV (ZnS) arasında değişir. Cd (II)'çe zengin nanotaneciklerin boyutu (4.4 nm), Zn (II)'çe zengin nanotaneciklerin boyutundan (3.1 nm) daha büyüktür. Sıcaklıkla kontrol

edilebilen silika duvarlarının kalınlığı $Cd_{1-x}Zn_xS$ nanotaneciklerin silika gözenekler içerisinde büyümesini sınırlar. Silika kanallarının boyutlarını 4.7 nm ve 3.3 nm arasında kontrol ederek CdS nanotaneciklerinin band aralıklarını 2.6 ve 2.8 eV arasında kontrol etmek mümkündür.

Anahtar Kelimeler: Mesoyapılı silika, iyonik olmayan yüzey aktifler, mesogözenekler, ageing, metal içeren sıvı kristaller, $Cd_{1-x}Zn_xS$ katı çözeltileri, nanotanecik, yarıiletken, bant aralığı.

ACKNOWLEDGEMENT

I would like to extend my gratitude to;

... Assoc. Prof. Dr. Ömer DAĞ for his encouragement and supervision throughout my studies…

…my family and my wife Gülçin, for their continuous support and help…

... Serhat, Serap, and Letice Günkan, for their hospitality…

…Çağrı Üzüm and Faik Demirörs, for their efforts in this project…

... Past and present members of Chemistry Department; where I learned a lot and made great friends during last 6 years.

TABLE OF CONTENTS

LIST OF TABLES

LIST OF FIGURES

1. INTRODUCTION

1.1 Liquid Crystals

The term liquid crystal implies a state of aggregation that is intermediate between the amorphous liquid and the crystalline solid. The first observations of liquid crystalline or mesomorphic behavior were made by Reinitzer and Lehmann in 1880th. Several thousands of organic compounds are known to form liquid crystals. They distinguish from liquids by the small degree of order among the molecules that destroys the isotropy of liquids (all directions are equivalent) and produces anisotropy (all directions are not equivalent). Solids can be either isotropic or anisotropic depending on the molecules occupying lattice sites and crystal lattice.[1] (Fig: 1.1)

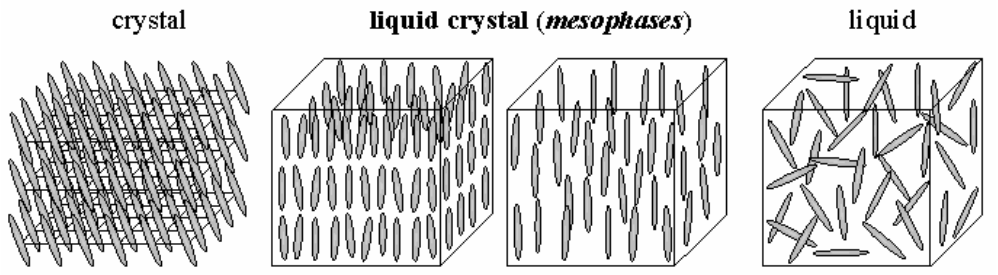

Fig.1.1. Representative of phase transition

Does a liquid crystal more resemble to a solid or a liquid? The amount of energy required to cause a phase transition is called the *latent heat* of transition and it is a useful measure of how different the two phases are. For example, the latent heat of the

cholesteryl myristate from solid to liquid crystal transition is 65 cal/g, while the latent heat for the liquid crystal to liquid transition is only 7 cal/g.[2] This smaller latent heat of the liquid crystal to liquid phase transition is evidence that liquid crystals are more similar to liquids than they are to solids. When a solid melts to a liquid crystal, most of the order of solid is lost, and retained small amount of order is lost at the liquid crystal to liquid phase transition.

The liquid crystal system passes through one or more mesophases before transforming into the liquid phase. These intermediate states may be brought by purely thermal processes (thermotropic liquid crystals, TLC) or by the influence of solvents (lyotropic liquid crystals, LLC). Temperature is the variable that determines which phase of matter exists for all of the TLC. Although temperature is still an important variable in determining the phase, the concentration of one component with respect to the other is far more important in the LLC systems. Through out this thesis work, we used LLC systems.

The lyotropic liquid crystals are made by mixing water with amphiphiles which are composed of hydrophobic and hydrophilic blocks. These blocks are covalently linked so microphase separation does not occur and the result is structured with dimensions on the order of 2-10 nm.[3] The ratio of water to surfactant determines the structure of the mesophase. If a small amount of surfactant is mixed with water, *micelle* and *vesicles* are formed according to strength of the polar head group of the surfactant molecules. If the surfactant molecules have a strong polar head group relative to the nonpolar part, they begin to arrange themselves into spheres with polar groups outside and the alkyl tail group toward the center. This structure is called a *micelle*. If the head group is not strong, the molecules form spherical *vesicles*, in which double layers of surfactant molecules form a shell with water inside and outside. Cross sections of vesicles and micelles are shown in Fig. 1.2 .

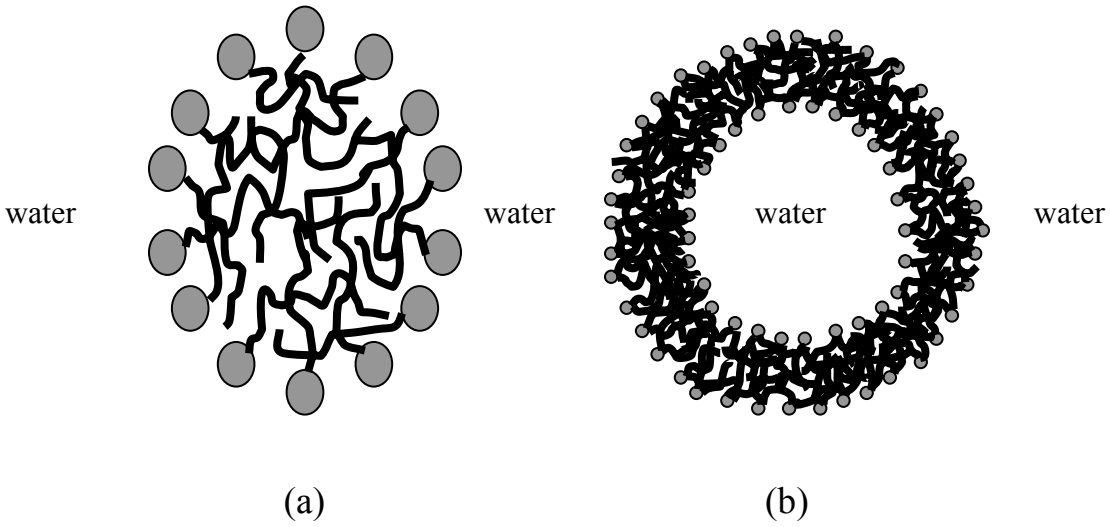

Fig.1.2. Cross sectional diagrams of two structures formed by amphiphilic molecules in water: (a) micelle and (b) vesicle.

If the concentration of surfactant material is increased, micelles or vesicles combine to form meso structures such as hexagonal mesophase, in which the long cylindrical rods of surfactant molecules arrange long rod axes in a hexagonal array. Another structure that forms at even higher concentrations is lamella mesophase in which the surfactant molecules form flat bilayers separated from each other by water. Fig. 1.3 shows the hexagonal and lamellar phases. A cubic mesophase forms at concentrations between the hexagonal and lamella mesophases.

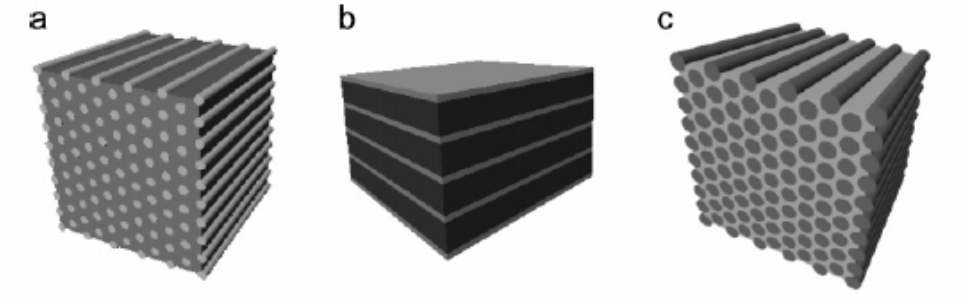

Fig.1.3. (a) hexagonal phase, (b) lamellar phase, and (c) inverse hexagonal phase. Hydrophilic domains are dark colored; hydrophobic domains are light colored.

Hydrophilic and hydrophobic domains of lyotropic liquid crystals may be used as nanoreactors due to their uniform arrangements in nanometer scale. By controlling liquid crystalline mesophase, it is possible to control the size, shape, connectivity, and dimensionality of these nanoreactors,[4] and also to control the size and shape of the nanoparticles formed inside them.[3] This synthesis mechanism is called template based synthesis mechanism. Inorganic materials copy the shape and the size of the organic templates.[5] In this study, hexagonal lyotropic liquid crystal mesophase has been used as a template for sculpting and shaping mesostructured materials.

1.2 Mesostructured Materials

Sol-gel chemistry and self-assembly procedures are used to control the texture of materials at nanometer scale.[6] The growth of soft chemistry, which is derived by inorganic and organized surfactant assemblies allowed to construct mesoscopic materials (2-50 nm); the best examples are mesostructured hybrids and mesoporous inorganic materials.[7]

Inorganic solids that contain pores with diameters in the size range of 20-500 Å are considered mesoporous materials.[8] Extremely high surface areas (> 1000 m^2g^{-1}) and precise tuning of pore sizes put these materials on the center of great interest in the field of nanomaterials.[9] Examples of mesoporous materials are: M41S family (16-100 Å), aerogels (> 100 Å), and pillared layered (10 Å, 100 Å) structures.

In the early 1990s, Kato[10] and Kresge from Mobil Research and Development Corporation[14] declared a new class of materials called FSM and MCM led to a new synthesis strategy for preparing mesoporous materials, respectively. Kato's and Kresge's groups used supramolecular templating to produce ordered mesoporous silica with high surface area and pore size, in the range of 2 to 10 nm. The M41S family was synthesized for the first time with regular, well-defined channels in a variety of pore sizes by the Mobil Research group. The liquid crystalline structures formed by the surfactant molecules have been used to assemble mesostructured silica. MCM-41 is the first reported example of mesoporous silica materials from M41S family that has 2D hexagonal pore arrangements.[11] Cubic, MCM-48 and lamella, MCM-50 are other members of the M41S family. (Fig.1.4)

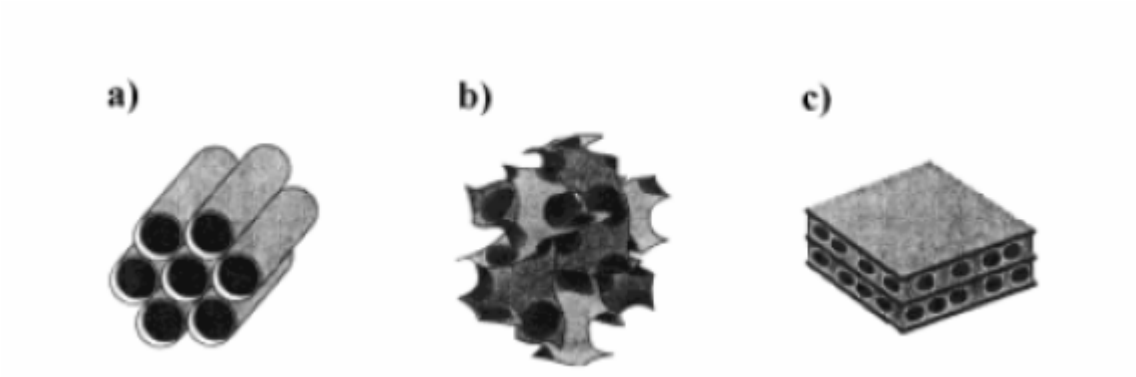

Fig.1.4. Members of mesoporous M41S materials, a)MCM-41, b)MCM-48, and c) MCM-50[12]

Over one decade, extensive research has been devoted to make more stable materials by expanding the pore size, extending the framework compositions, and examining new supramolecular templates. As a result, it is currently possible to produce

mesoporous materials with pore sizes from 2 to 50 nm,[13-14] and mesoporous transition metal oxides,[15-19] metal sulfides,[20-25] and hybrid silica/organic frameworks.[26- 29]

There have been a number of mechanisms proposed to explain the formation of mesoporous materials. In general, these mechanisms are based on the presence of surfactants and inorganic precursors (Fig.1.5). According to surfactant molecules concentration and hydrophilic-hydrophobic part lengths, different mesoporous materials are formed with inorganic precursor's interaction. The metal salts can be used as inorganic precursors to synthesis mesostructured host. Therefore, metal ions can locate easily inside the mesopores to form nanosized materials.

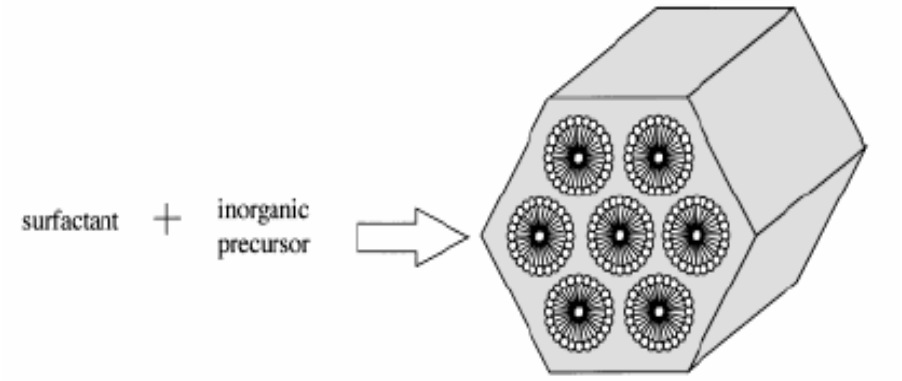

Fig.1.5. Representation of the general formation of MCM-41 from inorganic precursors and organic surfactants.

1.3 Nanosized Materials

Synthesis of nanosized materials has become an important research field because these materials have particular optical and electronic properties, which differ significantly from their bulk materials. Low dimensional materials, including zero dimensional

quantum dots and one dimensional quantum wires, have attracted special attention because of size quantization effects and potential applications in optoelectronics. Some physical properties, such as enhanced local field effects for metals,[30] quantum confinement for semiconductors,[31] are observed from nanocrystals, smaller than 10 nm. The quantum confinement effect describes how the electronic and optical properties change when the size of materials are smaller than 10 nm. When the length of a semiconductor is reduced below exciton Bohr radius, the quantum confinement effects are observed. The exciton is an electron-hole pair, existing in a material and the distance between the electron and hole within the exciton is called exciton Bohr radius (i.e., a few nanometers). The quantum confinement effect arises in semiconductors when excitons are confined by a potential well in 1D (quantum well), 2D (quantum wire), or 3D (quantum dot). A quantum well is a structure where the size of one direction is comparable with the Bohr exciton radius while the exciton can move freely in other two directions. In quantum wire structure, sizes of two directions are about the Bohr exciton radius, and a quantum dot is a structure where all dimensions are near the Bohr exciton radius, so the exciton can not move freely in quantum dot structure. Therefore, the physical properties of nanocrystals strongly depend on their size, shape, surface state, and arrangement of nanoparticles.

Despite the wide applications of such materials, controlling the particle dimensions can be one of the major problems. For instance, aggregation of nanoparticles and the difficulty of controlling their morphology are known problems.[32-33] In order to prevent aggregation, nanoparticles have previously been covered with a protective layer (mono or multi layer films[34-35]) or have been attached to a variety of support materials (microemulsion,[36] sol-gel,[37-38] or polymer[39-41]). Using solid support as a medium for nanoparticle formation has been shown to stabilize the particles and to control their growth.

1.4 Sol-Gel Processes of Silica

Preparation of silica by the sol-gel process usually involves use of a silicon alkoxide. The resultant microstructures of silica gels depend on the concentration of reactants, reaction temperatures, water to alkoxide mol ratios and acidity or basicity of the catalyst. Various starting compounds have been used to prepare silica gels. The most frequently used starting materials are silicic acid, and alkoxysilanes; particularly tetramethoxysilicate (TMOS) and tetraethoxysilicate (TEOS).

In the polymerization reaction, condensation starts as soon as the alkoxy group has been hydrolyzed (Fig. 1.6); silicon-oxygen-silicon bonds are formed immediately after addition of water and catalyst,[42] because initial polymerization around hydrolyzed alkoxysilane molecules is quite fast. At a later stage, further polymerization is possible with cross-linking of chains which are separated from one another by alcohol and water molecules. The cross-linking of those chains eventually leads to gel formation.

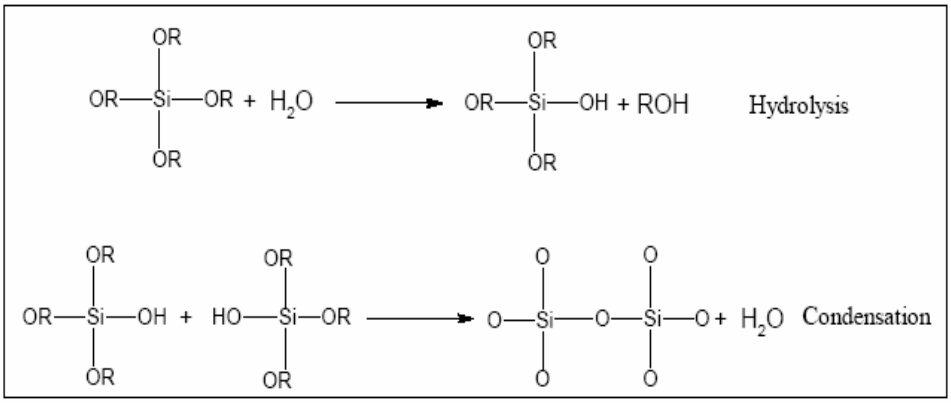

Fig.1.6. Hydrolysis and condensation reactions of silica oxide.

1.5 Mesoporous Silica as Host Materials

Periodic mesoporous silica materials are one of the most important materials to support nanocrystals. These mesoporous materials can be used as molds to obtain nanocrystals with controlled size and shape. Support materials are prepared using surfactants as structure directing agents. The second step of the process is to modify the internal surface of these support materials. There is a rapidly growing interest in modification methods to produce new functional materials.[11] Chemical vapor deposition,[43] ion- exchange,[44-45] impregnation,[46-47] liquid crystalline templating (LCT),[48-49] functionalizing pore walls with organic groups,[50] doping mesopores with quantum dots,[51] etc. are some methods for modifying mesoporous silica materials. Drug delivery systems,[52] synthesis of optical materials,[44, 53-54] synthesis of polymers,[55] monolayer depositions of thiols,[56] encapsulation of metal ions and metal nanoclusters,[51, 52-62] etc. are some examples for the modified mesoporous silica materials. Mesoporous silica materials also offer various morphologies such as thin films,[63] powders,[64] and monoliths,[48] for this purpose. There are many studies concerning growth of nanoparticles in the channels of mesoporous powders.[43, 65-70] However, in these structures, the particles are usually randomly distributed within the pores where their sizes are not well controlled. Only few studies have reported synthesis of periodic arrays of nanoparticles with rather small domains.[71-72] Synthesis of nanowires inside mesoporous powders has also been reported.[72-73]

For optical applications, it would be better to organize nanoparticle arrays in the film samples instead of the powder samples. Mesoporous silica films are of special interest because of their wide application in optics and electronics, such as lasers[74-75] sensors,[76] and photochromic films.[77] Since mesoporous silica materials are rigid solids, it has to be shaped into thin films at the post synthesis stage. Dip coating provides the means to obtain high quality films. Evaporation induced self-assembly process is basis of the formation of thin films in the dip coating method. Evaporation of the co-solvent at the interface between liquid and air results in concentration of the non-volatile species,

formation of surfactant micelle species and followed by their self-assembly with the silica species.[78]

Many of the mesopores silica films have regular porous structure. However the structural control on macroscopic scale is difficult. Several parameters have been examined to control the alignment of tubular mesopores in mesoporous silica such as reactant flow,[79-80] shearing,[81] strong magnetic field,[82] and using various substrates with surface structural anisotropy.[83-86] Mesoporous silica thin films are potentially excellent hosts for semiconductor structures because of their high degree of order and large band-gap of silica which serves as a barrier material between the nanoparticles.

Synthesis of mesopores silica films using LLC mesophase as a templating media was first reported by Attard *et al.*[48] They have used nonionic surfactants (C_nEO_m) in their LLC mesophase to produce mesopores silica films and monoliths. Some advantages of using non-ionic surfactants over the ionic surfactants are: thicker inorganic walls, easy tuning of pore diameter and easy removal of surfactant molecules.[7,31] Note also that the phase diagrams of the surfactant/silica/water system at high surfactant concentration are similar to the phase diagram of surfactant/water alone. Attard's method is also known as liquid crystalline templating (LCT) method that uses nonionic surfactants, water and tetramethyl orthosilicate (TMOS). The mixture is a liquid at early stages of the mixing. However, hydrolysis of TMOS, condensation of silica species and evaporation of methanol (hydrolysis side product) and some of water molecules reforms the LC mesophase after a short period of time (5-10 min). Further polymerization of this silicatropic LC mesophase causes the transition from LC phase to mesostructured solid phase.

1.6 Lyotropic LC system of Salt: Surfactants and Synthesis of Transition Metal ions Modified Mesostructured Silica

Water and surfactant molecules form binary LLC mesostructures which originates from weak intermolecular forces such as van der Waals, dipole-dipole interactions and hydrogen bonding. Small amount of metal salts could be added to the binary system as a third component without a phase separation or a LC phase collapse. The variation in components concentration, salt content, pH and temperature affect stability and structure of the mesophase.

However, some transition metal aqua complex salts could be dissolved in surfactant molecules and induce the surfactants to undergo self-assembly into a LC mesophase without water. Advantage of this salt/surfactant binary system is that one can introduce large amount of salts without destroying the LC mesophase. Dag et. al.[87] reported that assemblies formed between the non-ionic oligo-(ethylene oxide) surfactants $C_{12}H_{25}$-$(CH_2CH_2O)_{10}OH$ and transition metals aqua complex salts have LC mesophase at various salt/surfactant ratios. Influence of transition metal salt ions to the LC phase has been extensively studied.[87-90]

The new lyotropic liquid crystalline (LLC) phase can be formed using oligo-(ethylene oxide) surfactants (C_nEO_m)[87] or Pluronics ($EO_xPO_yEO_x$)[91] and some transition metal aqua complex salts $[M(H_2O)_x]Y_2$ (where M is some of the first and second row transition metal ions and Y is NO_3^-, Cl^-, and ClO_4^- counteranions).[87-90] In the new system, different transition-metal salts could be dissolved in water free C_nEO_m, or in water-C_nEO_m systems to obtain the LC mesophase. The type and concentration of the metal salts and interactions of metal aqua complex ion-surfactant and metal ion-counteranion collectively induce a self assembly into hexagonal or cubic mesophases.

The salt-surfactant system is liquid at low salt concentration (0.5-1.2 salt:surfactant mole ratios), hexagonal between 1.2 and 3.2 and cubic phase is observed at

higher salt concentrations (above 3.2 mol ratios).[87] Addition of water to the salt: surfactant system affects structure of the LLC mesophase. For instance a mixture of water:salt:surfactant at low salt concentrations (salt/surfactant mole ratio below 1.2) is liquid crystalline that collapses upon water evaporation. At higher salt concentrations, the mixture is in liquid phase and evaporation of excess water leads to an ordered mesophase.[90] In both systems, salt-surfactant and water-salt-surfactant systems, free water in the LLC and coordinated water (M-OH_2) in the new systems[49] mediates the self-assembly processes.

In all these organizations, Hofmeister's series (SO_4^{2-} > HPO_4^{2-} > CrO_4^{-} > CO_3^{2-} > Cl^- > Br^- > NO_3^- > I^- > ClO_4^- > SCN^-) is effective. Anions on the left-hand side of the series are lyotropic and make surfactant molecules more hydrophobic; anions on the right hand side are hydrotropic and make the surfactant molecules more hydrophilic. Therefore, metal salts of lyotropic anions should be less soluble in surfactant, such as SO_4^{2-}, and Cl^- salts are not soluble in C_nEO_m nonionic surfactants.[87] Dag et. al.[89] demonstrated that transition metal perchlorate salts are less soluble than nitrate salts in a salt:surfactant LC system despite of the Hofmeister's series. Coordination of nitrate ion to metal ion center plays an important role in this observation.[89]

Nitrate ions exist as coordinated and free in the mixture. The coordination of nitrate ion reduces the symmetry of free nitrate ion from D_{3h} to C_{2v} such that stretching mode of free ions splits into two. The spectral changes show that free and coordinated nitrate ions have an equilibrium (1).

$$[M(H_2O)_n]^{2+} + 2NO_3^- \leftrightarrow [M(H_2O)_{n-1}(NO_3)]^+ + NO_3^- + H_2O \qquad (1)$$

At low water concentration, the equilibrium shifts to right and nitrate ions coordinate to metal center. It makes the complex ion +1 charged rather than +2 charged in the free ion case. Coordination of nitrate anions to metal ions reduces ionic strength of medium and it prevents crystallization of the salt in the LC medium. Consequently, position of anions in the medium determines the LC phase stability and structure.

However, in presence of silica species, the LC mesophase appears at relatively low salt concentrations. For example, the LC mesophase of a $[Cd(H_2O)_4](NO_3)_2$-$C_{12}EO_{10}$ appears at a ~ 1.20 mole ratio with a hexagonal structure,[92] but in presence of silica species, the LC mesophase exist at even 0.0 mole ratio. The 2D and 3D hexagonal mesophases are observed in the nitrate salt systems at low salt concentrations.

Addition of silica sources to a mixture of water-salt-surfactant LC phase, a metal ion containing silicatropic LC mesophase forms with hydrolysis and condensation reactions in this media, which eventually goes to a solid phase to form mesostructured silica. Therefore, addition of transition metal ion can be handled at the first step of the process. With complete silica polymerization, the structure becomes stable and can be used as a rigid template for production of nanoparticle.

1.7 $Cd_{1-x}Zn_xS$ Nanoparticles

Synthesis and characterization of semiconductors are of great interest for both fundamental research and technical applications. There are many novel properties due to large number of surface atoms and three-dimensional confinement of electrons in nanocrystalline semiconductors.[93-98] By changing size of particles, degree of confinement of electrons changes and this affects electronic structure of the solid, especially band gaps of the semiconductors.

Among various semiconductor materials, binary metal chalcogenides of group IIB have been the most studied due to their potential applications. They have nonlinear optical and luminescence properties,[93-101] quantum size effect,[93-104] and other important physical and chemical properties.[105-110] For example; nanocrystalline thin films of CdS and ZnS are attractive materials in photoconducting cells and optoelectronic devices such as solar cells and photodetectors.[111-112] Also, relevant ternary compound $Cd_{1-x}Zn_xS$ is a

wide band gap semiconductor. It has various potential applications such as high density optical recording devices, blue or even ultraviolet laser diodes, and photovoltaic cells.[113-114] These applications are based on the quantum-well structures of $Cd_{1-x}Zn_xS$ which show adsorption edges changing from green to UV.[115]

It is well established that well-controlled size and shape can be achieved by controlling thermodynamics and kinetics during nucleation and growth of nanocrystals.[116-117] A good control, at the nucleation and growth stages, is one of the most necessary conditions for producing high quality nanocrystals. If the nucleation and growth of nanocrystals occurs at same time, product will have a broad size distribution. One of the methods to separate these two stages is to achieve one pot synthesis without precursor injection method.[118] Cao *et al*. demonstrated the nanocrystals nucleation and growth stages separation in a homogeneous system with the presence of nucleation initiators.

There are different techniques for preparation of CdS nanoparticles such as ionic reactions in liquids,[95,114] gas-liquid precipitation,[119] and solid state reactions.[120] Qian and co-workers developed a solvothermal method to synthesize CdS.[121-122] Thermolysis of single source precursor is also an important method to synthesize metal sulfide nanocrystals.[124-125] Zhong and co-workers reported a new facile chemical route to size controllable high quality CdS, ZnS and $Cd_{1-x}Zn_xS$ nanocrystals by using one-pot method in high boiling point long chain amines at high temperatures.[125] Low temperature synthesis of group II-VI semiconductor provided several advantages.[126] As an example, Parkin *et al.* developed a liquid ammonia method to synthesize metal chalcogenides at room temperature.[127] There are still some limitations by using these methods to synthesize semiconductor nanoparticles. For example, dissatisfying photoluminescence quantum yields, broad particle size distributions or toxic, unstable and pyrophoric agents were employed such as H_2S, $(TMS)_2S$ or $Cd(CH_3)_2$.

Several media such as dispersed media,[128] reverse micelles,[129] and vesicles[128] have been used to form $Cd_{1-x}Zn_xS$ ternary alloys at room temperature. When nanoparticles are capped inside a dielectric matrix, quantum confinement may be achieved with attractive optical properties and narrow size distributions can be achieved.[130] For this reason, several groups have studied these techniques. For example, Atta *et al*.[131] used sol gel technique for the preparation of microcrystalline CdS and (Cd, Zn)S doped titania films to study their optical absorption and fluorescence properties, Padam *et al.*[132] reported structural, optical and electrical properties of solution grown thin films of $Cd_{1-x}Zn_xS$ and B. Bhattachrjee *et al.*[130] reported the $Cd_{1-x}Zn_xS$ nanocrystals in the silica thin film matrix. There are few groups investigating synthesis of CdS nanoparticles in channels of mesopores materials. The methods used ion-exchange or impregnation methods that involve reaction under H_2S gas.[133-134] Zhang et al[135] described a method of assembling nanoparticles inside the mesopores of externally functionalized silica MCM-41 materials through the metal ions transportation via ion-exchange reactions. In this method, SiO^- is an anion on the nanopore surface and surfactant ions are cationic and organized in the form of a cylindrical micellar structure. They have weak Coulombic interaction that can be easily broken by another cation through ion exchange. Therefore, the surfactant ions can be used to transport metal ions inside the mesopores while the external surface is capped with hydrophobic phenyl group to prevent the possibility of adsorption of hydrophilic metal ions on the external surfaces during the ion-exchange reaction. In the final step, treatment with H_2S produced the CdS nanoparticles inside the MCM-41 powder (Fig.1.7). Average diameter of the CdS nanoparticles is less than 2.5 nm and pore diameter is around 3.6 nm.

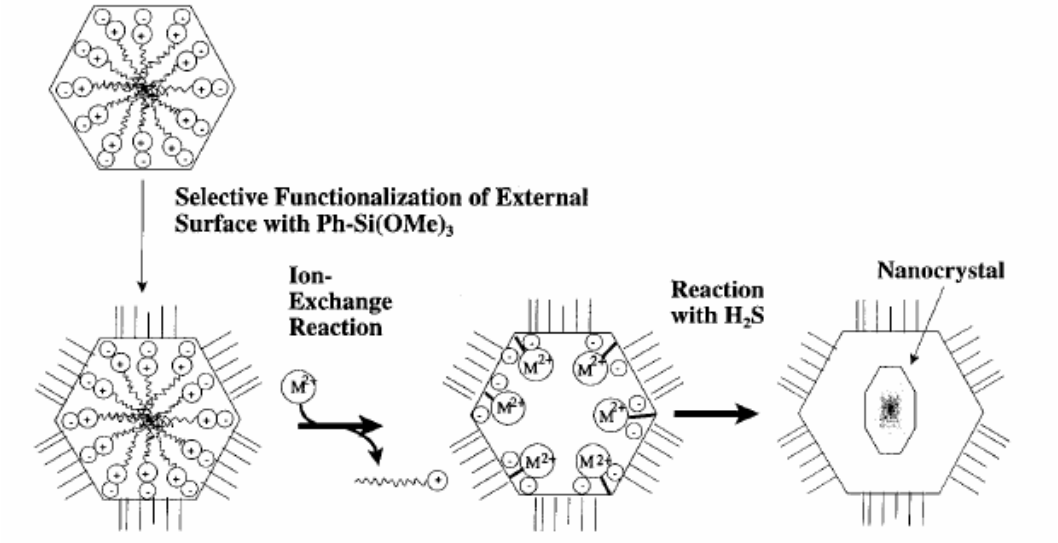

Fig.1.7 The schematic diagram of ion-exchange reaction and CdS formation.

Besson *et al*.[46] synthesized the CdS nanoparticles within the channels of mesopores silica films with impregnation method. These films have open pores that allow different solutions to fill by impregnation method. The films were calcined at 450^0C to remove the surfactant molecules to obtain highly ordered hexagonal films. The cadmium ions were introduced with a basic solution of cadmium nitrate and they were adsorbed on silica walls (cationic metal and $Si\text{-}O^-$ interaction) that form the internal surface. Diffusion of the H_2S into the film precipitates the metal ions to metal sulfides nanoparticles eventually fills the silica pores. To obtain saturated silica pores with CdS nanoparticles, impregnation and precipitation were repeated several times. The formation of nanoparticles inside the silica pores are usually monitored by UV-visible and XRD techniques.

Nanosized ZnS has also been synthesized in the channels of MCM-41 materials by using surface modification methods.[43] The pure mesoporous silica sample was obtained by calcination at 540^0 C. Functional groups (ethylenediamine groups) were introduced to the pore surfaces of mesoporous silica and the resulting hybrid materials absorbed the

Zn^{2+} ions in water and ethanol solutions. After reaction with H_2S, nanosized ZnS (< 2.5 nm) was produced in the channels of MCM-41 powder.

In this thesis, the $Cd_{1-x}Zn_xS$ nanocrystals were synthesized in the channels of mesostructured silica films. Our template mechanism is built by the extension of lyotropic liquid crystalline (LLC) mesophase with a new metal ion containing liquid crystalline (MLC) mesophase[87-90] that consists of transition metal salts (TMS) and nonionic surfactants, C_nEO_m. (Fig.1.8) We have added the Cd^{2+} and Zn^{2+} ions to the synthesis mixture where the metal ions contribute to the template formation. They locate within the mesopores and form nanocrystals after reaction with H_2S. Therefore, we do not need any additional methods such as ion-exchange, impregnation and surface modification to transfer the metal ions into the channels of mesoporous silica films. Other methods need many reaction steps and auxiliaries to synthesize the nanosized materials; however, MLC technique consists of only two steps and does not need many auxiliaries to synthesize $Cd_{1-x}Zn_xS$ nanocrystals.

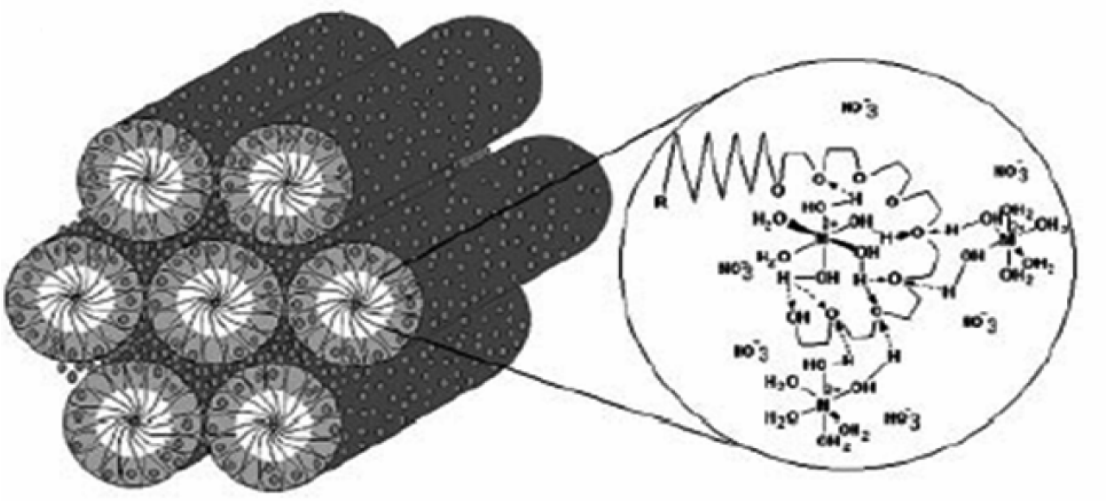

Fig.1.8. A schematic representation of a hexagonal LC structure, the small circles represent $[M(H_2O)_n]^{2+}$ and NO_3^- ions.

In this assembly process, a mixture of surfactant, acid (as a catalyst), TMOS (as a silica source), and water first produces a liquid mixture, then with hydrolysis and condensation of the silica source liquid mixture is transformed to LC mesophase. Finally, a solid phase by maintaining the structure of the LC mesophase forms. In this system, coordinated water molecules, M-OH_2, organize the self-assembly process as Si-OH in the silicatropic and M-OH in the other metallotropic systems.[136-137] The LLC and MLC approach collectively allow us to incorporate large amounts of transition metal ions into mesopores. This method has advantages for controlling the morphology, transparency and concentration of nanocrystals in the mesostructured silica materials.

This method allows incorporation of more than one type of transition metal ions at once, such that the compositional flexibility can be introduced into the final materials. The other advantage of the mechanism is structural flexibility in the final material by controlling the structure of the MLC mesophase. Varying the salt concentration, ionic-strength and the type of counter anion in the media[49,90] controls the structure of MLC mesophase. For example, transition metal salts with nonionic surfactants, C_nEO_m produce a 2D hexagonal mesophase; however 2D hexagonal structure changes to 3D hexagonal mesophase with increasing the water concentrations.[90] Counter anion also determines the structure of the mesophase. For example, perchlorate salts usually produce cubic mesophase, whereas nitrate salts usually produce hexagonal mesophase.[90] Therefore, preparing metal ion containing liquid crystalline mesophase with composition of Cd / Zn mol ratio from zero to infinity enables us to control;

1-The homogeneous distributions of Cd^{2+} and Zn^{2+} ions in channels of the mesostructured silica films.

2-The structure of the mesostructured silica films.

3-The composition of the $Cd_{1-x}Zn_xS$ nanoparticles after exposing the silica films to H_2S gas.

2. EXPERIMENTAL

2.1 Materials

All chemicals and solvents were reagent grade and used as received without any further treatment.

Surfactants used throughout this work, homogeneous polyoxyethylene 10 lauryl ether, $CH_3(CH_2)_{11}(OCH_2CH_2)_{10}OH$, (designated as $C_{12}EO_{10}$, M_w=626.862 g/mol) is commercially available from Aldrich, Germany and the triblock copolymer having a poly(ethylene oxide)-poly(propylene oxide)-poly(ethylene oxide) (EO-PO-EO) so called Pluronics, P123 ($PEO_{20}PPO_{70}PEO_{20}$, M_w =5800 g/mol) was donated by BASF Corp. and used without further treatment.

Salts, cadmium(II) nitrate tetrahydrate ($[Cd(H_2O)_4](NO_3)_2$), and zinc(II) nitrate hexahydrate ($[Zn(H_2O)_6](NO_3)_2$), were obtained from Aldrich, Germany. Concentrated nitric acid HNO_3 (70 %), silica source, tetramethylorthosilicate (TMOS, %99 pure) and hydrogen sulfide (H_2S, 99.5 % pure) were also obtained from Aldrich, Germany.

2.2 Synthesis

2.2.1 Synthesis of Mesostructured Silica Templates

Various amounts, respectively, moles of 1-x and x (x is between 0.0 and 1.0) of the $[Cd(H_2O)_4](NO_3)_2$ and $[Zn(H_2O)_6](NO_3)_2$ salts were dissolved in 3 ml of H_2O that was acidified by 0.10 grams of concentrated nitric acid (70 %). To this mixture, first 1.00 gram of $C_{12}EO_{10}$ (1.595×10^{-3} mol) and then 1.60 grams of TMOS (1.05×10^{-2} mol) were added at once. Either gentle heating or simple shaking homogenized the resulting liquid mixture in 30 minutes. Thin film samples were prepared by dip coating with a coating speed of 0.4 mm/s over a glass, quartz and silicon surfaces for various measurements. The thick film samples were prepared by spreading the mixture over the surfaces of microscope slides for POM and XRD measurements at high angles. The Cd^{2+} and Zn^{2+} containing mesostructured materials were prepared by varying the Zn^{2+}/Cd^{2+} and $M^{2+}/C_{12}EO_{10}$ (M = Zn and Cd) mole ratios from 0.0 to and 1.0, respectively. The mesostructured silica thin films were aged in the oven at various temperatures (RT-250^0 C) for various times (Discussed in detail in the results and discussion section).

In the case of Pluronic (P123) surfactant, the preparation route is similar. However, a mixture of TMOS, water, acid, and surfactant (P123) with a composition of 1.6 g: 3.0 g: 0.1 g: 1.0 g, respectively and 3.0 mole ratio of salt:surfactant. P123 is more difficult to homogenize than the $C_{12}EO_{10}$ surfactant. Therefore, the mixture was stirred to homogenize by a magnetic stirrer before and after the TMOS addition. The clear solution was either dip coated on glass slides or casted over glass slides and investigated by XRD and UV-Vis absorption spectroscopy.

2.2.2 Synthesis of $Cd_{1-x}Zn_xS$ nanoparticles

The thin film and thick samples were reacted in an evacuated reaction chamber under 150-200 torrs of H_2S gas for 5 and 10 minutes, respectively. This process usually produces stable transparent nano-$Cd_{1-x}Zn_xS$-meso-SiO_2 composite materials with yellow color in the Cd(II) rich samples and colorless at Zn(II) rich samples. The film samples were then washed using water/ethanol (1:1 v/v) solution to prevent the degradation of the $Cd_{1-x}Zn_xS$ nanoparticles in the channels of silica host.

2.2.3 Calcination of the nano-CdS-meso-SiO_2

The thin film samples of nano-CdS-meso-SiO_2 material were aged at 170^0 C for 15 minutes and then calcined by heating from 25°C to 450°C in 5 hours and kept at 450°C for 5 hours in a temperature controlled oven. Then, the samples were cooled to measure the XRD patterns, UV-Vis and FTIR spectra.

2.3 Instrumentation

2.3.1 Polarized optical microscopy

Polarized optical microscopy (POM) images were obtained in transmittance mode on a Meije Techno ML9400 series Polarising Microscope with transmitted light illumination, using convergent white light between the parallel and crossed polarizer. The POM images have been used to characterize the mesophases formed from salt:surfactant:silica systems.

2.3.2 X-Ray Diffraction

X-ray diffraction (XRD) patterns were recorded on a Rigaku Miniflex diffractometer using a high power Cu-K_α source operating at 30kV/15mA. The XRD

patterns were recorded in low and high angle regions to monitor both the mesophase and $Cd_{1-x}Zn_xS$ nanocrystals, respectively. Both the thin films and thick films were prepared on glass and silicon surfaces. The XRD patterns of a sample were collected at least twice in the 1-5, 2θ range with a scan rate of 0.80^0/minute. The high angle diffraction patterns of some samples were also recorded between 15-60^0, 2θ values with a scan rate of 0.50^0 /minute.

2.3.3 UV-VIS Spectra

UV-VIS Spectra were recorded using a Varian Cary 5 double beam spectrophotometer with a 100 nm/min speed and a resolution of 2 nm over a wavelength range, from 800 to 200 nm. The UV-Vis absorption spectra were obtained from the film samples of nano-$Cd_{1-x}Zn_xS$-meso-SiO_2 materials over glass and quartz slides.

.

2.3.4 FT-IR Spectra

FT-IR spectra were recorded with a Bruker Tensor 27 model FTIR spectrometer. A DigiTect^{TM} DLATGS detector was used with a resolution of 4 cm^{-1} and 64 scans for all samples. The FTIR spectra were recorded as thin films on a single Si (100) wafer.

2.3.5 TEM Images

TEM images were recorded on a Hitachi HD-2000 STEM operating at 200kV and 30mA and a Philips 430 microscope with an accelerating voltage of 120 kV. The samples were prepared by dispersing the powder/fragments onto a carbon film-supported 200 mesh copper grid or embedded in epoxy resin and microtomed.

2.3.6 ^{29}Si MAS-NMR

^{29}Si MAS-NMR (magic angle spinning nuclear magnetic resonance) proton coupled spectra were recorded using a Bruker DSX 400 spectrometer. Samples were spun at 5000 Hz, the chemical shift values were reported with respect to tetramethylsilane (TMS).

3. Results and Discussion

3.1 Synthesis of Mesostructured Silica Templates

In this thesis, thin film of mesostructured silica was used as a template for the synthesis of metal sulfide nanoparticles. Metal Containing Liquid Crystalline (MLC) media was used to prepare the mesostructured silica films. Salts ($[Zn(H_2O)_6](NO_3)_2$, and $[Cd(H_2O)_4](NO_3)_2$), surfactant ($C_{12}EO_{10}$) and water form liquid crystalline mesophases. The salt:surfactant mole ratio is important to create stable lyotropic liquid crystalline mesophase as thin films. In the binary salt:surfactant systems, salts' hydrate ions interact with surfactant hydrophilic groups and form LC mesophases. Therefore, salt amount must be adequate to form the mesophase. If water is added to the salt:surfactant medium, the LC mesophase form even at low salt-surfactant mole ratio, however, evaporation of the water collapses the mesophase at low salt concentrations.

$[Cd(H_2O)_4](NO_3)_2$, (CdX_2) and $[Zn(H_2O)_6](NO_3)_2$, (ZnX_2) salts are optically anisotropic when dissolved in C_nEO_{10} surfactants between the ranges of 1.4-3.2 and 1.2-3.4, salt/surfactant mole ratios, respectively.[87] Above these mole ratios, they form isotropic cubic mesophase. The change from hexagonal to cubic phase is a result of equilibrium between hydrophilic and hydrophobic domains.[87]

In order to preserve the LC mesophase as a thin film, we have added silica to the salt:surfactant media that has a salt:surfactant mole ratio of 1.0. Silica species are hydrophilic and assist the salt ions in their interactions with the surfactant molecules. Therefore, despite the water evaporation from the thin film, the polar silica oligomers preserve the LC mesophase. In addition to the hydrophilic effect of the silica species, polymerization with time stabilizes the mesostructure. In this assembly process, the LC mesostructured thin film transforms to solid mesostructured thin film by the hydrolysis

and condensation reactions of TMOS. Nitric acid was used as a catalyst for the silica polymerization reaction. To obtain a highly polymerized silica wall, surrounding the mesopores, the thin films were aged at RT for a long time (1 day to 1 week) and at higher temperatures for shorter time. Ageing process causes further polymerization of the silica walls of the films.

The silica species are hydrophilic and increase the hydophilicity of the media in a salt:surfactant system. At low salt concentrations, the mixture produces 3D hexagonal mesostructured silica. However, the anisotropic mesophase disappears at around a salt to surfactant mole ratio of 1.25 in salt:surfactant silica system.[49] Therefore, we optimized the reaction composition by changing the salt:surfactant mole ratio in our synthesis media. A composition of 1.6 g: 3.0 g: 0.1 g: 1.0 g TMOS, water, acid, and surfactant, respectively and 1.0 mole ratio of salt:surfactant produces good quality film samples, which were characterized using POM and XRD techniques.

Anisotropic LC materials have usually two different indices of refraction that allow us to observe optical textures between crossed polarizers. The polarized optical microscopy is a common technique used to determine the structure of LC mesophases. For example, 2D and 3D hexagonal LC phases produce different focal conic fan textures between crossed polarizers. On the other hand, isotropic cubic LC phases do not produce any kind of texture, and its POM image is completely dark.

The silica samples obtained from the $[Zn(H_2O)_6](NO_3)_2$,(ZnX_2), $[Cd(H_2O)_4](NO_3)_2$,(CdX_2), and $Cd_{0.5}Zn_{0.5}X_2$: $C_{12}EO_{10}$: water : TMOS : HNO_3 mixtures display 3D hexagonal fan texture at 1.0 mole ratio of salt/surfactant upon ageing for 1 day. Fig. 3.1.1 shows the POM images of ZnX_2-meso-SiO_2, CdX_2-meso-SiO_2 and $Cd_{0.5}Zn_{0.5}X_2$-meso-SiO_2 samples. All the images are characteristic of the 3D hexagonal mesostructure.

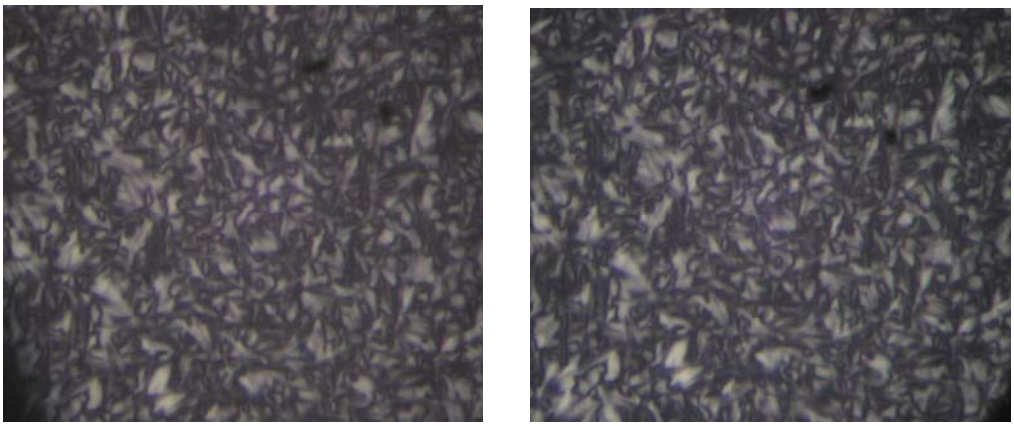

(a) **(b)**

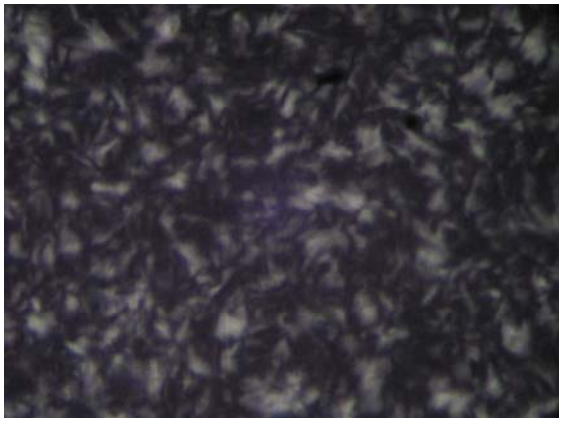

(c)

Fig.3.1.1. The POM images of a) ZnX_2-meso-SiO_2, b) CdX_2-meso-SiO_2 and c) $Cd_{0.5}Zn_{0.5}X_2$-meso-SiO_2.

To complement and further analyze the structure of the film samples, X-ray diffraction method has also been applied. The XRD method is another powerful technique to identify the structure of mesostructured materials. Usually, these materials have diffraction lines at low angles, between 1 and 10^0, 2θ. The hexagonal (2D and 3D), cubic and lamellar structures are the mostly observed structure types in mesostructured silica materials. Bragg's Law formalizes the XRD principle, and d-spacing values can be

obtained using Bragg's equation. Fig. 3.1.2 shows the diffraction of X-rays and Bragg's law.

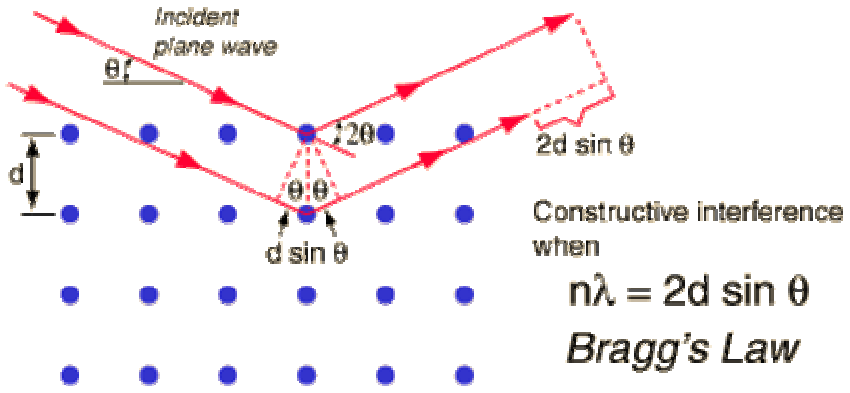

Fig. 3.1.2. Diffraction of X-Rays and Bragg's Law
(λ: wavelength, d: the spacing of the layers, θ: the incident angle of the photons).

The silica materials used in this work have a 3D hexagonal structure. The 3D hexagonal structure displays diffraction lines, connected to the following relationship (where d is d-spacing, h, k, l are reflection indices, and **a** and **c** are unit cell parameters).

$$1/d^2 = 4/3(h^2+hk+k^2)/a^2 + l^2/c^2 \qquad (1)$$

The 3D hexagonal structure has a linear correlation in a plot of d spacing versus $(8/(10.667(h^2+hk+k^2)+3l^2))^{1/2}$. The slope of this plot gives **a** parameter with a zero intercept. Fig.3.1.3 displays a plot of the relation between d spacing values of the first four planes in the 3D hexagonal structure and h, k, l relation. The unit cell parameter **a** is 59.6 Å, and **c** is 97.3 Å with a *c/a* = 1.632 with a space group of $P6_3$ mm. These are all consistent with 3D hexagonal structure.

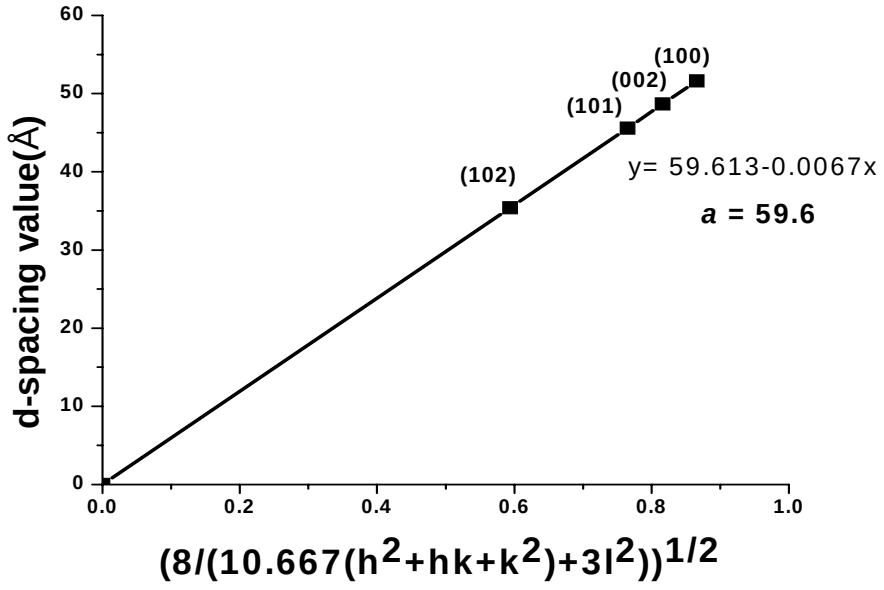

Fig.3.1.3 A plot of linear relation between d-spacing and $(8/(10.667(h^2+hk+k^2)+3l^2))^{1/2}$.

The film samples are usually oriented in one direction and the diffraction planes along these directions dominate to the diffraction pattern. Therefore, we measured the diffraction patterns of the oriented film samples at different orientations to determine the structure of the silica host, Figure 3.1.4 (A) and (B). Figure 3.1.4 (A) and (B) show the characteristic 3D hexagonal XRD patterns with 5 diffraction lines between 1.5 and 5.0, 2θ range, indexed to (100), (002), (101), (102), and (110) lines at 51.6, 48.6, 45.6 and 35.4, 29.8 Å d spacings, respectively.

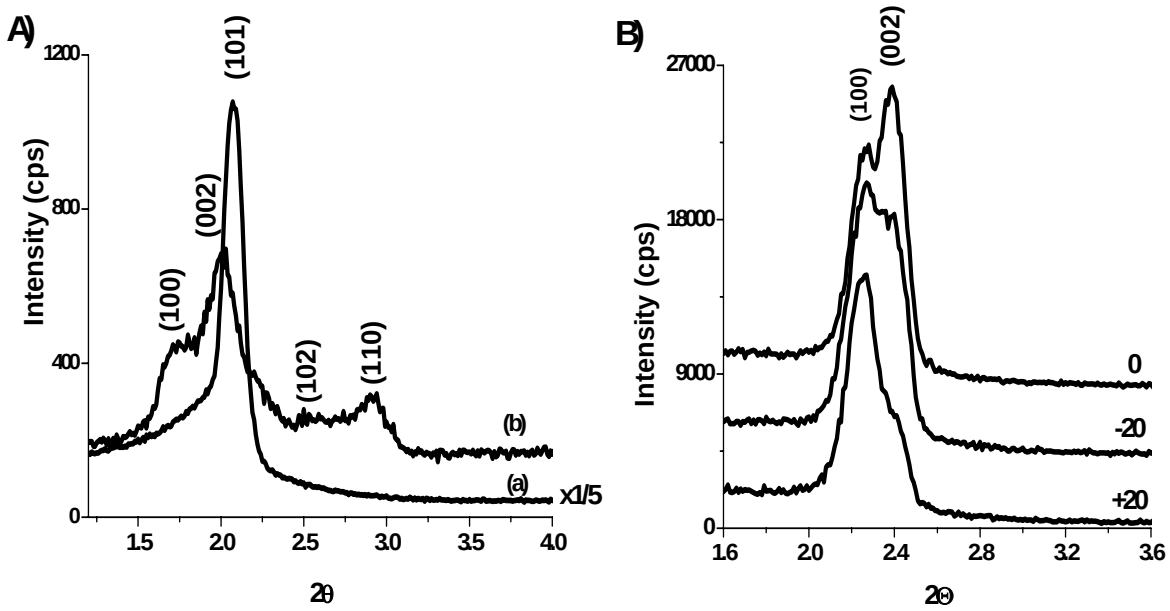

Fig. 3.1.4. The XRD patterns of A) (a) $[M(H_2O)n](NO_3)_2$-meso-SiO_2 film and (b) powder samples, B) Oriented thick and aged at high temperature $[M(H_2O)_n](NO_3)_2$-meso-SiO_2 film sample recorded at three different orientations.

The reason of seeing one diffraction line in the thin film's XRD pattern (Fig.3.1.4.A-(a)) is the orientation in (100) or in some cases in (101) directions during the film making process. Therefore, measurements at different orientations with respect to the incident beam reveal the other plane of the structure (see Figure 3.1.5). In Figure 3.1.4 (B), the measurements were recorded in three different orientations. Rotating the samples from $+20^0$ positions to the zero position, the intensity of (100) line goes down while the intensity of (002) line goes up, Figure 3.1.5. Another way to observe these diffraction lines is to run the powder form of the samples. Crashing the films or monoliths destroys the initial orientations. However, this reduces the intensities of all diffraction lines, Fig. 3.1.4 (A). The XRD and POM results collectively reveal that the $[M(H_2O)_n](NO_3)_2$-meso-SiO_2 (M= Zn and Cd) materials have 3D hexagonal structure. Figure 3.1.6 shows typical XRD patterns of thin film of $[M(H_2O)_n](NO_3)_2$-meso-SiO_2 (where M is Zn(II), Cd(II), mixed Cd(II)-Zn(II) and salt:surfactant mole ratio of 1.0). The film samples are oriented and display only one diffraction line at 1.80^0.

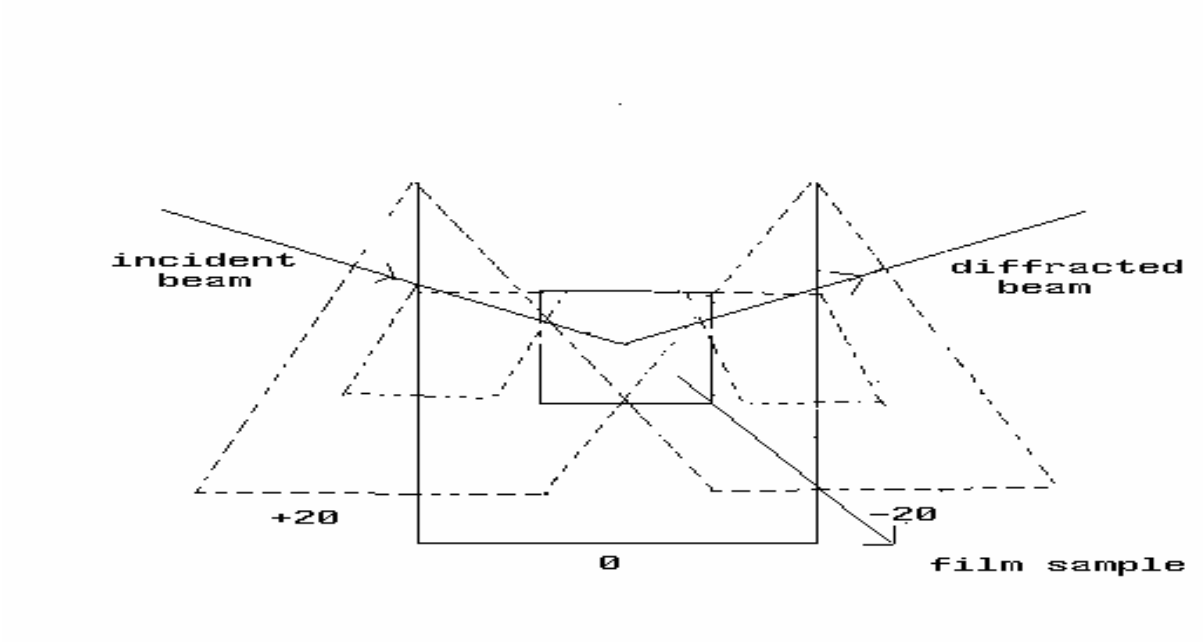

Fig. 3.1.5. Rotating the film samples from $+20^0$ position to -20^0 position.

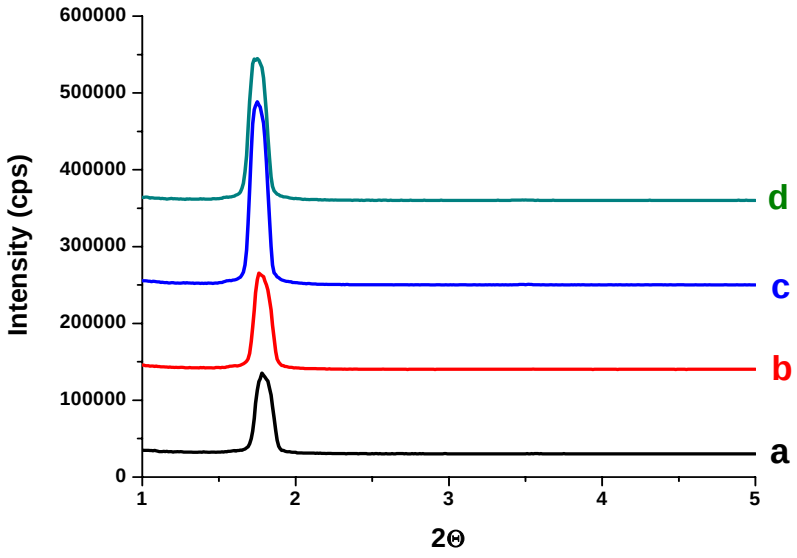

Fig.3.1.6. The XRD patterns of a) $[Cd(H_2O)_4](NO_3)_2$-meso-SiO_2

b) $([Cd(H_2O)_4](NO_3)_2)_{0.7}$-$([Zn(H_2O)_6](NO_3)_2)_{0.3}$-meso-$SiO_2$

c) $([Cd(H_2O)_4](NO_3)_2)_{0.4}$-$([Zn(H_2O)_6](NO_3)_2)_{0.6}$-meso-$SiO_2$

d) $[Zn(H_2O)_6](NO_3)_2$-meso-SiO_2.

In this thesis, we worked with two types of materials, fresh and aged thin films. Thin films were aged with time at room temperature (RT) or at high temperatures to enhance silica polymerization and to obtain rigid silica walls. Ageing process has an important effect in producing nanocrystals because mesostructured silica becomes rigid that limits the growth of nanoparticles. XRD patterns of aged (at RT) thin films of $([Cd(H_2O)_4](NO_3)_2)_{0.5}$-$([Zn(H_2O)_6](NO_3)_2)_{0.5}$-meso-$SiO_2$ and $[Zn(H_2O)_2](NO_3)_2$-meso-SiO_2 are shown in Figure 3.1.7. They all have similar diffraction patterns at low angles. The silica polymerization at RT up to two days did not change the pore diameter, (4.7 nm).

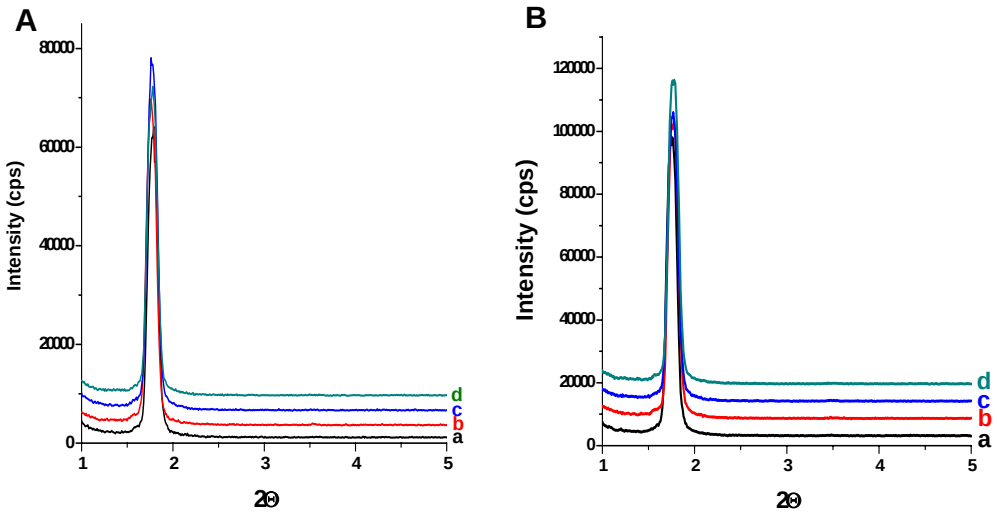

Fig.3.1.7. The XRD patterns of **(A)** $([Cd(H_2O)_4](NO_3)_2)_{0.5}$-$([Zn(H_2O)_6](NO_3)_2)_{0.5}$-meso-$SiO_2$ after ageing at RT a) 1 hour, b) 4 hours, c) 1 day, d) 2 days. **(B)** $[Zn(H_2O)_2](NO_3)_2$-meso-SiO_2 after ageing at RT a) 1 hour, b) 4 hours, c) 1 day, d) 2 days.

In hexagonal structure, the d-spacing corresponding to (100) planes give an idea about the pore size. Figure 3.1.8 shows a schematic diagram of a unit cell. The thickness of the silica wall is about 1.0 nm[48]. The relation below can be used to estimate the pore size in these materials.

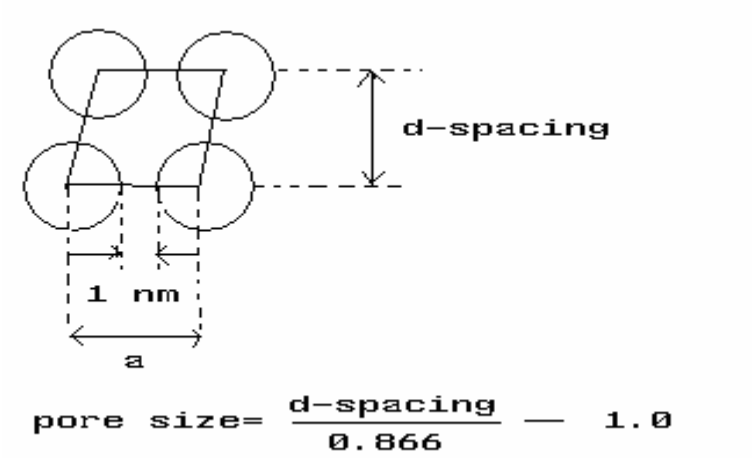

Fig. 3.1.8. Schematic representation of a relation between d-spacing and pore size.

However, heating the films at higher temperatures shrinks the pores due to further condensation of SiOH groups. Figure 3.1.9 shows the XRD patterns of the $[Cd(H_2O)_4](NO_3)_2$-meso-SiO_2 samples that were aged at 100^0 C from 30 minutes to 3 days. The diffraction line shifts from 1.87^0 (Figure 3.1.9(a)) to 2.12^0 (Figure 3.1.9(e)) as a result pore size decrease from 4.5 nm to 3.8 nm upon ageing at 100^0 C for 2 days.

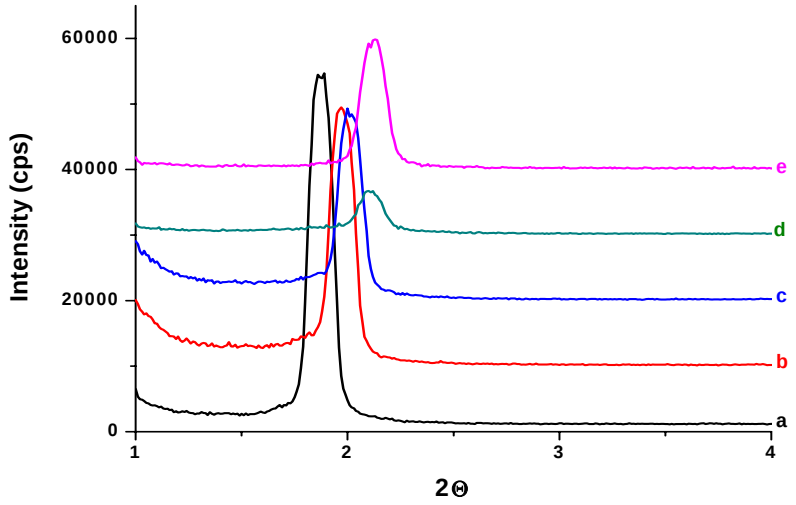

Fig. 3.1.9. The XRD patterns of $[Cd(H_2O)_4](NO_3)_2$-meso-SiO_2 after ageing at 100^0C a) 30 minutes b) 3 hours, c) 5 hours, d) 1 day e)2 days.

The silica condensation constantly shrinks the silica walls until it collapses at higher temperatures. As a result, the diffraction line shifts to higher angles and disappears above 250^0C. Figure 3.1.10 shows the diffraction patterns between 1.2^0 and 3^0, 2θ, at various temperature of a $[Cd(H_2O)_4](NO_3)_2$-meso-SiO_2 film sample. The diffraction line shifts from 1.8^0 to 2.4^0 corresponding to a pore size decrease from 4.7 nm to 3.3 nm due to heating from RT to 240^0C.

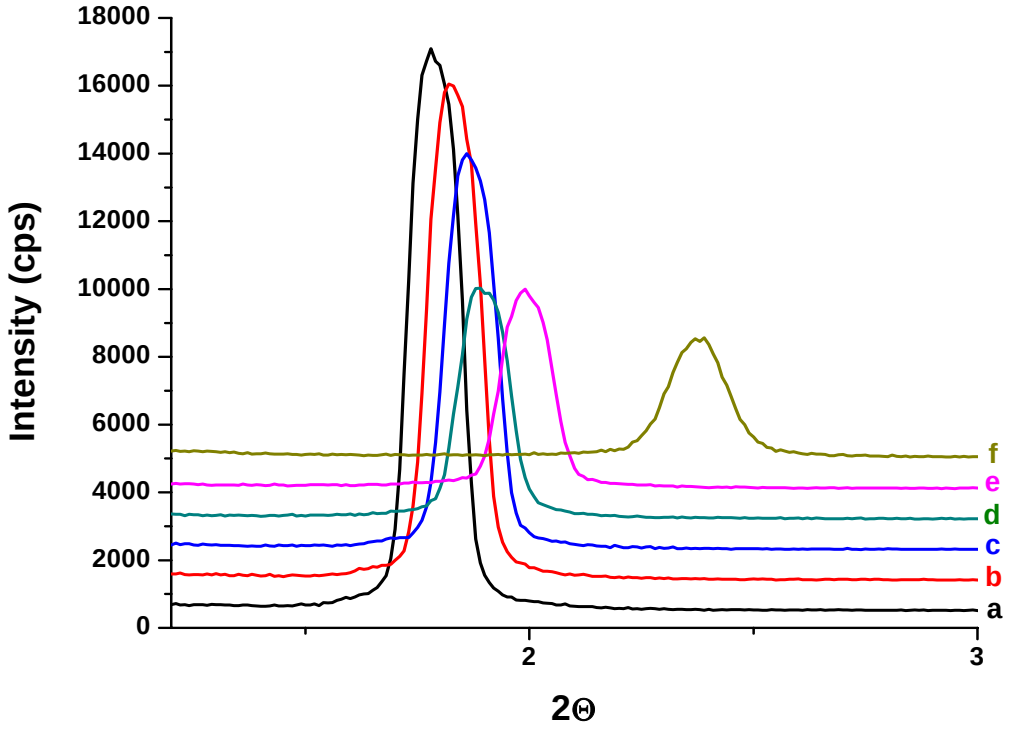

Fig. 3.1.10. The XRD patterns of $[Cd(H_2O)_4](NO_3)_2$-meso-SiO_2 film sample after ageing at a) RT, b) 50^0C, c)100^0C, d)150^0C, e) 200^0C, and f) 240^0C.

The mesostructured silica film samples have further investigated using ^{29}Si Magic Angle Spinning Nuclear Magnetic Resonance (MAS-NMR) Spectroscopy. Fig. 3.1.11 shows a series of ^{29}Si MAS-NMR spectra of aged samples (RT, 100^oC and 240^oC). The ^{29}Si MAS-NMR spectra of the samples display 3 peaks at δ -91, -101, and -110 with respect to TMS due to **Si**$(OH)_2(OSi)_2$ (Q_2), and **Si**$(OH)(OSi)_3$ (Q_3) and **Si**$(OSi)_4$ (Q_4)

units, respectively. The trend in the spectra shows that Q_4 band at -110 ppm increases in intensity with increasing temperature indicating further condensation of the silanol groups. Q_2 band at -90 ppm is decreasing due to further condensation of silanol groups at higher temperatures. Q_2 and Q_3 bands transform to Q_4 band with ageing samples.

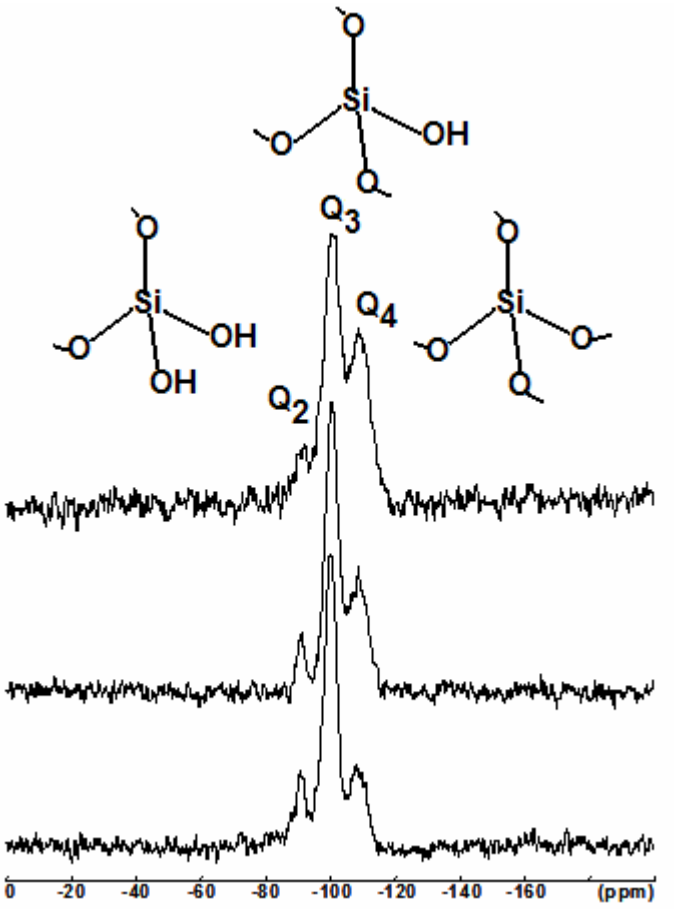

Fig.3.1.11. The ^{29}Si-MAS NMR of $[Cd(H_2O)_4](NO_3)_2$-meso-SiO_2 samples aged at RT (bottom), 100^{o}C (middle) and 240^{o}C (top).

3.2 Synthesis of CdS, ZnS and $Cd_{1-x}Zn_xS$ in Mesostructured Silica Films

3.2.1 POM, TEM, EDX and XRD Analysis

The metal ions of Cd(II) and Zn(II) inside the silica channels react with hydrogen sulfide gas (H_2S) to form CdS, ZnS and $Cd_{1-x}Zn_xS$ nanoparticles. The thin film samples were reacted in an evacuated reaction chamber under 150-200 torrs of H_2S gas to produce stable transparent film (represented as nano-$Cd_{1-x}Zn_xS$-meso-SiO_2) composite materials (where x is from 0.0 to 1.0).

The H_2S gas pressure and exposure time collectively affect the nanocrystals formation in the film samples. Deep coating method provides very thin films so we do not need high pressure of H_2S gas for its diffusion to all parts of the sample. 150-200 torrs of pressure was enough to obtain transparent nano-$Cd_{1-x}Zn_xS$-meso-SiO_2 film samples. The top layer of the film reacts with H_2S immediately, however layers under the surface react with H_2S relatively slow. Therefore, the thin films were exposed to gas for 5 minutes and thicker films were exposed for 10 minutes. If the samples were exposed to gas for long time, sulfur (S_8) formation was observed in the thicker films.

The film samples display the same POM image due to 3D hexagonal mesostructured silica before and after H_2S treatment. Figure 3.2.1 shows two representative POM images of nano-$Cd_{0.5}Zn_{0.5}S$-meso-SiO_2 and nano-ZnS-meso-SiO_2 of mesostructured silica films. The 3D hexagonal mesostructure was preserved after nanoparticle formation inside the silica channels.

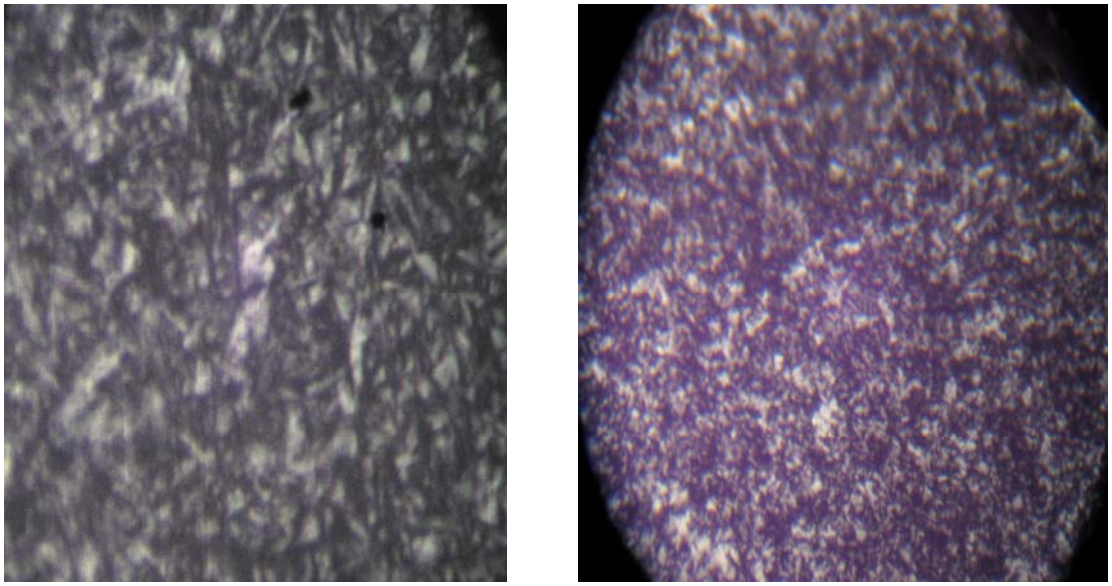

(a) **(b)**

Fig.3.2.1. The POM images of a) nano-ZnS-meso-SiO_2, and b) nano-$Cd_{0.5}Zn_{0.5}S$-meso-SiO_2 mesostructured silica film.

Tunneling Electron Microscopy (TEM) can be used to obtain images of the samples in nanometer scale. Bright-field imaging and dark-field imaging methods are two most common TEM imaging methods. Bright-field images are constructed using the direct electrons, while dark-field images use the diffracted electrons. In the bright-field imaging, regions of the sample that scatter many electrons, like defects such as dislocations, look darker. With dark-field images, strongly diffracting regions look brighter. Figure 3.2.2 shows two TEM images of nano-$Cd_{1-x}Zn_xS$-meso-SiO_2 and nano-CdS-meso-SiO_2 film samples. Figure 3.2.2 (A) shows a bright field image of a portion of a nano-$Cd_{0.5}Zn_{0.5}S$-meso-SiO_2 film sample. The $Cd_{1-x}Zn_xS$ nanoparticles are indicated as darker spots of sub-micron size (100 nm = 0.1 μ). Figure 3.2.2 (B) clearly shows that these sub-micron spots are composed of small nanoparticles that are around 4 nm. Figure 3.2.2 (B) displays images due to oriented silica channels and $Cd_{0.5}Zn_{0.5}S$ nanoparticles inside the channels of mesostructured silica. The H_2S reactions carried over fresh samples

due to soft nature of silica walls causes pore enlargement of the partially polymerized silica walls of the channels. This is clearly visible in the image in Figure 3.2.2 (B). The parts with nanoparticles are larger than the parts with no nanoparticles. The XRD and UV-Vis data also correlate this enlargement of the pore size during the H_2S reaction in the fresh samples.

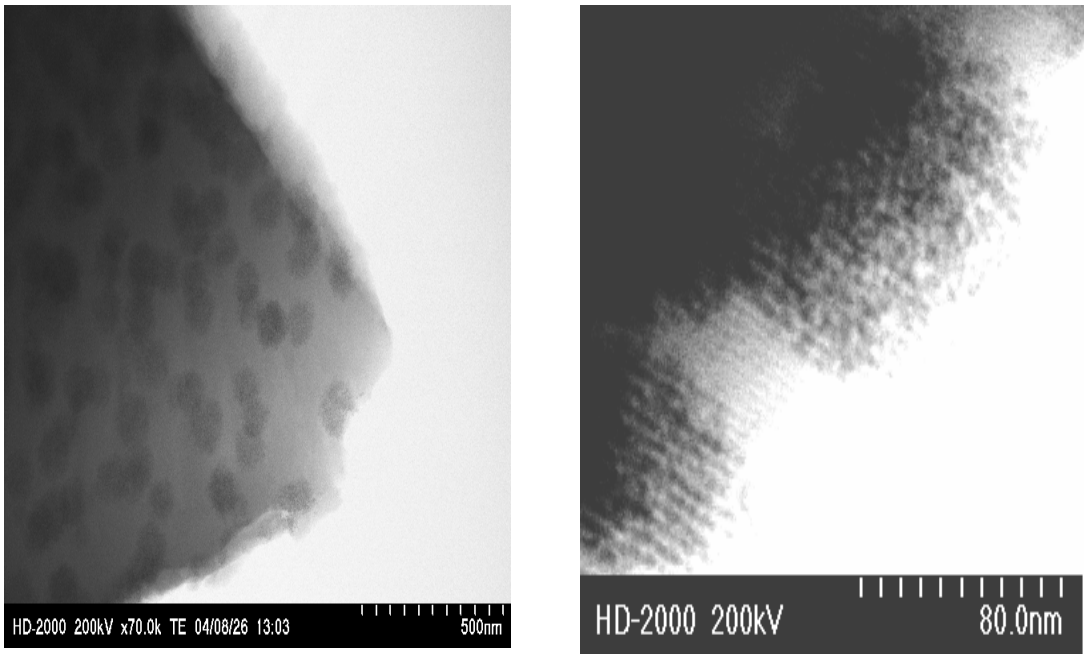

(A) **(B)**

Fig. 3.2.2. The TEM images of thin film samples; **A)** a bright field (scale bar is 500 nm) and **B)** a bright field image (scale bar is 80 nm) of nano-$Cd_{0.5}Zn_{0.5}S$-meso-SiO_2.

Fig. 3.2.3 (A) and (B) show dark field and bright field images of nano-$Cd_{0.3}Zn_{0.7}S$-meso-SiO_2 and nano-CdS-meso-SiO_2, respectively, obtained from aged samples. The light spots correspond the $Cd_{0.3}Zn_{0.7}S$ nanoparticles in the silica channels, Figure 3.2.3 (A). The homogeneously distributed $Cd_{0.3}Zn_{0.7}S$ nanoparticles with uniform size distribution in the silica matrix are shown in Fig. 3.2.3 (A). The nanoparticles are smaller, around 3 nm, than in the fresh samples, Fig. 3.2.2 (B). The origin of this is shrinking of the silica pores, due to further condensation of silica walls in the aged samples. The results

obtained from TEM images are also consistent with the XRD and UV-Vis data (see later).

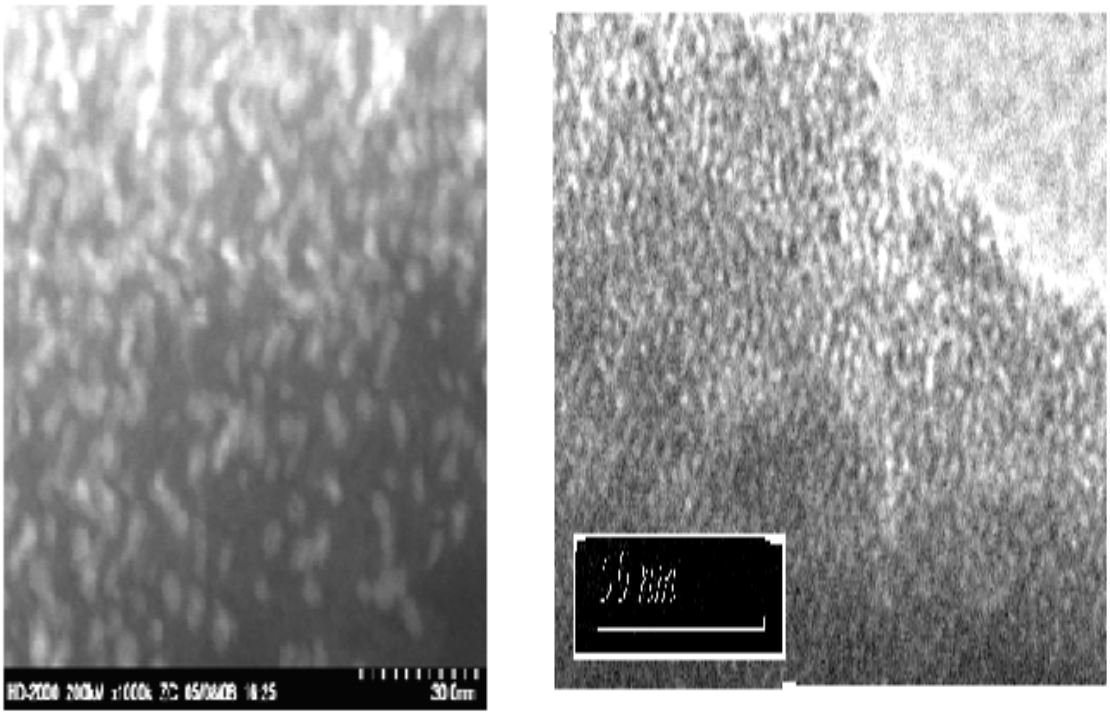

(A) **(B)**

Fig. 3.2.3. The TEM images of thin film samples A) a dark field image of nano-$Cd_{0.3}Zn_{0.7}S$-meso-SiO_2 (scale bar is 30 nm) and B) a bright field image of an aged sample of nano-CdS-meso-SiO_2 (scale bar is 50 nm).

In order to understand whether all Cd(II) and Zn(II) ions react with H_2S or not, we used Energy Dispersive X-ray (EDX) analysis method. It is sometimes referred to also as EDS or EDAX analysis. It is a technique used for identifying the elemental composition of samples. During the EDX analysis, sample is bombarded with an electron beam and so the inner shell electron is ejected. An outer shell electron occupies this vacancy and excess energy is emitted as X-ray. The atom of every element releases X-rays with unique amounts of energy; therefore, the identity of the atom from which the X–ray was emitted can be established. The EDX spectrum is just a plot of how frequently an X-ray

is produced for each energy level and normally it displays peaks corresponding to the energy levels for which the most X-rays were received. Each of these peaks is unique to an atom so corresponds to a single element. The highest peak in the spectrum is the more concentrated element in the sample.

Fig. 3.2.4 shows EDX spectra and weight percentage of chemical composition of nano-CdS-meso-SiO_2 and nano-$Cd_{0.7}Zn_{0.3}S$-meso-SiO_2 film samples. EDX spectrum of nano-$Cd_{0.7}Zn_{0.3}S$-meso-SiO_2 shows the initial salt ratios of Cd^{2+} and Zn^{2+} as 7/3 and the total salt concentration is equal to sulfur concentration. In the EDX spectrum of nano-CdS-meso-SiO_2, the Cd^{2+} ion/sulfur mole ratio is also around one. It is important to conclude that all metal ions react with H_2S and produce CdS, ZnS and $Cd_{1-x}Zn_xS$ nanoparticles according to initial salt types and amounts. Carbon, oxygen and silica atoms have also peaks in EDX spectrum, due to surfactant molecules and silica framework of the film samples.

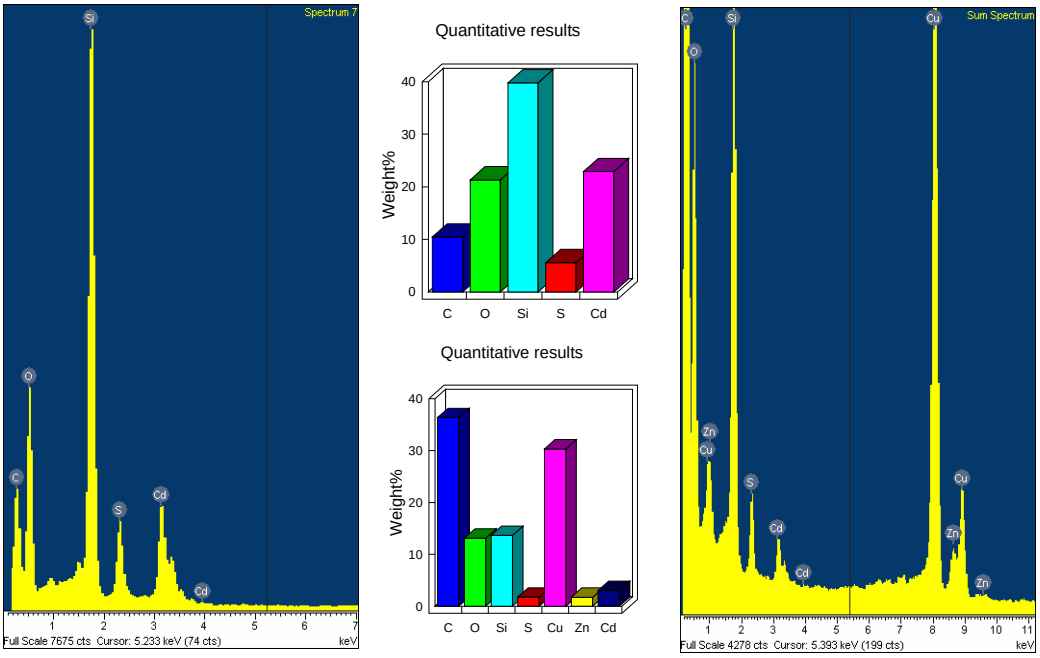

Fig. 3.2.4. The EDX spectra and quantitative elemental analysis of nano-CdS-meso-SiO_2, left and top and nano-$Cd_{0.7}Zn_{0.3}S$-meso-SiO_2, right and bottom, respectively.

The XRD patterns of the $[M(H_2O)_n](NO_3)_2$-meso-SiO_2 (where M is Zn(II), Cd(II) and mixed Cd(II)/Zn(II)) before and after H_2S treatment are shown in Figure 3.2.5. After H_2S reaction, the sharp diffraction line becomes broad and shifts to a lower angle (around 1.60^0). It indicates that the pore diameter increases from 4.7 nm to 5.5 nm because of the formation of $Cd_{1-x}Zn_xS$ nanoparticles inside the silica channels. However, if the film samples were aged at higher temperatures, the silica walls resist the growth of the nanoparticles. The aged samples do not display any shift upon H_2S treatment. This will be further discussed in section 3.3

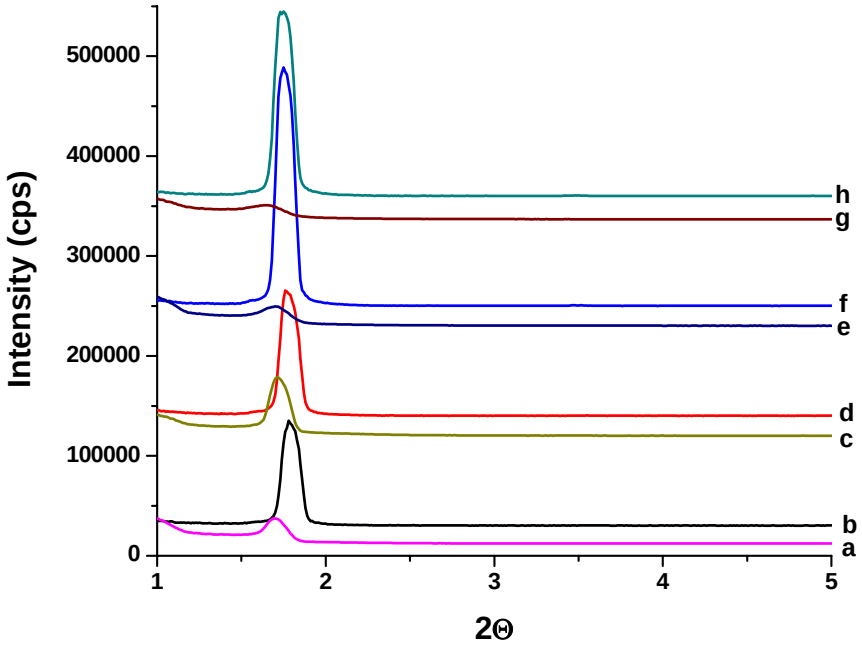

Fig.3.2.5. The XRD patterns obtained from fresh film samples of a) nano-CdS-meso-SiO_2 b) $[Cd(H_2O)_4](NO_3)_2$-meso-SiO_2 c) nano-$Cd_{0.7}Zn_{0.3}S$-meso-SiO_2 d) $([Cd(H_2O)_4](NO_3)_2)_{0.7}$-$([Zn(H_2O)_6](NO_3)_2)_{0.3}$-meso-$SiO_2$ e) nano-$Cd_{0.4}Zn_{0.6}S$-meso-SiO_2 f) $([Cd(H_2O)_4](NO_3)_2)_{0.4}$-$([Zn(H_2O)_6](NO_3)_2)_{0.6}$-meso-$SiO_2$ g) nano-ZnS-meso-SiO_2 h) $[Zn(H_2O)_6](NO_3)_2$-meso-SiO_2.

3.2.2 HIGH ANGLES XRD ANALYSIS OF $Cd_{1-x}Zn_xS$ NANOPARTICLES

The high angle XRD patterns were also recorded to obtain structure and unit cell parameters of the $Cd_{1-x}Zn_xS$ nanocrystals. In order to observe the diffraction lines, relatively thicker film samples were prepared on silicon (Si) wafers to improve the signal to noise ratio. The Si (200) diffraction line detected at 32.96^0, 2θ, is used as a reference to obtain the correct diffraction angles. The XRD patterns of $Cd_{1-x}Zn_xS$-meso-SiO_2 in the high angle region displays changes depending on the Cd(II)/Zn(II) initial mole ratio. Figure 3.2.6 shows the XRD patterns of the $Cd_{1-x}Zn_xS$-meso-SiO_2 samples. All the diffraction lines index well with zinc blend structure for all compositions. The unit cell parameter **a** calculated using all diffraction lines and equation (2) changes linearly from 5.84 Å to 5.42 Å going from CdS to ZnS.

$$1/d^2=(h^2+k^2+l^2)/a^2 \qquad (2)$$

The CdS, ZnS and $Cd_{1-x}Zn_xS$ nanoparticles have cubic zinc blend structures. The diffraction lines due to (111), (220) and (311) planes of CdS are observed at 26.41^0, 44.00^0, and 52.60^0, respectively from the nano-CdS-meso-SiO_2 materials. These diffraction lines shift to higher angles, 28.45, 47.60, 56.40^0, and broaden going from CdS to ZnS in the $Cd_{1-x}Zn_xS$ nanocrystals.

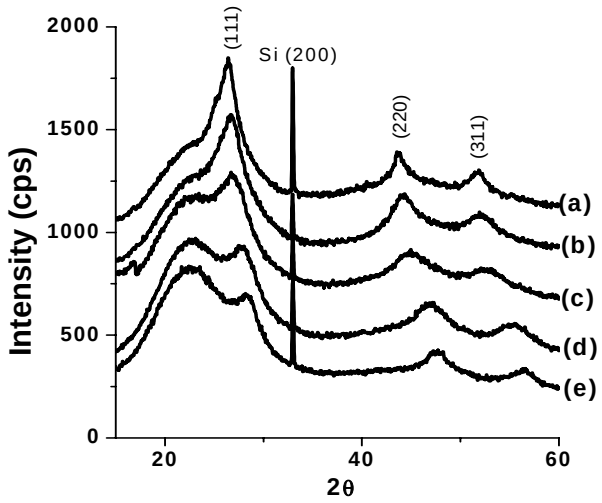

Fig.3.2.6. The XRD patterns of nano-$Cd_{1-x}Zn_xS$-meso-SiO_2 of mesostructured silica films, where x is (a) 0.00, (b) 0.25, (c) 0.5, (d) 0.85 and (e) 1.00. The sharp line at 32.96^o is due to Si substrate (used as an internal reference).

Figure 3.2.7 shows a linear dependence of the unit cell parameter on the composition of the nanocrystals. The unit cell parameter of CdS nanocrystals is around 5.82 Å and for ZnS nanocrystals, it is around 5.42 Å. Other nanocrystals, $Cd_{1-x}Zn_xS$, when x is 0.25, 0.5, 0.75 and 0.85, have unit cell parameters between the two end systems and their unit cell sizes linearly depend on initial salt ratio. This indicates that nanocrystals are forming a solid-solution in the nano-$Cd_{1-x}Zn_xS$-meso-SiO_2 films.

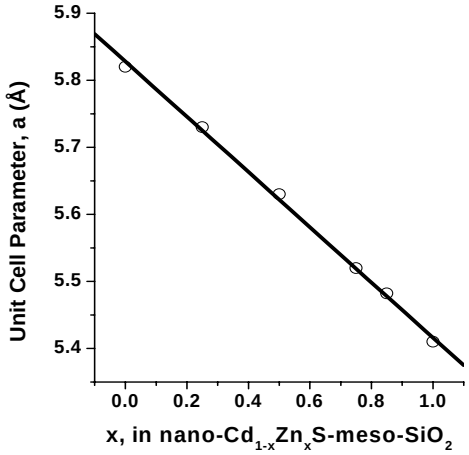

Fig.3.2.7 A plot of the unit cell parameters evaluated from the XRD patterns in Fig.3.2.6 versus composition, x in nano-$Cd_{1-x}Zn_xS$-meso-SiO_2

The XRD data also provides the particle size of the nanocrystals using Scherrer's formula,

$$D=0,9\lambda/ B\cos\theta \qquad (3)$$

where D is the diameter of the particles in Å, λ is wavelength of the X-ray source, 1.54078 Å, B is the corrected full width at half maximum in radian and θ is half of the angle of diffraction of the (111) plane. The particle size of $Cd_{1-x}Zn_xS$ nanocrystals that was obtained from Scherrer's formula is around 4.0 nm, and it is consistent with the values obtained from TEM images and UV-Vis absorption (see the text below).

3.2.3 UV-Vis ABSORPTION ANALYSIS OF $Cd_{1-x}Zn_xS$ NANOPARTICLES

The electronic absorption spectra of the nano-$Cd_{1-x}Zn_xS$-meso-SiO_2 samples were recorded in transmittance mode using thin films on quartz and glass substrates. The UV-Vis absorption spectroscopy is one of the most sensitive techniques to determine optical band gaps of semiconductor nanoparticles. The band gap values of semiconductor nanocrystalline materials are higher than semiconductor bulk values due to quantum confinement effect and the absorption-edge of the nano-CdS-meso-SiO_2 blue shifts going to nano-ZnS-meso-SiO_2. The bulk band gap values of CdS and ZnS are 2.42 eV and 3.68 eV, respectively[130]. The band gaps for each sample were evaluated using the linear fit of the absorption edge after plotting the spectra against $(A^* h\upsilon)^2$ versus $h\upsilon$[49]. This relation is valid for direct band gap materials. Note that both CdS and ZnS are direct-band gap semiconductors.

Figure 3.2.8 shows absorption spectra of the nano-$Cd_{1-x}Zn_xS$-meso-SiO_2 samples. The absorption edges of CdS and ZnS start at 495 and 314 nm, respectively. The other nanocrystals, (where x is between 0.0 and 1.0) absorption edges are between 495 and 314 nm. The absorption-edge gradually blue shifts going from CdS to ZnS nanocrystals. The observed sharp absorption edges indicate that the $Cd_{1-x}Zn_xS$ nanoparticles in the channels of mesostructured silica materials have a uniform size distribution. The direct band gap

fit of the absorption edges gives 2.6 eV for pure CdS, 3.2 eV for $Cd_{0.5}Zn_{0.5}S$ and 4.1 eV for pure ZnS in Figure 3.2.9.

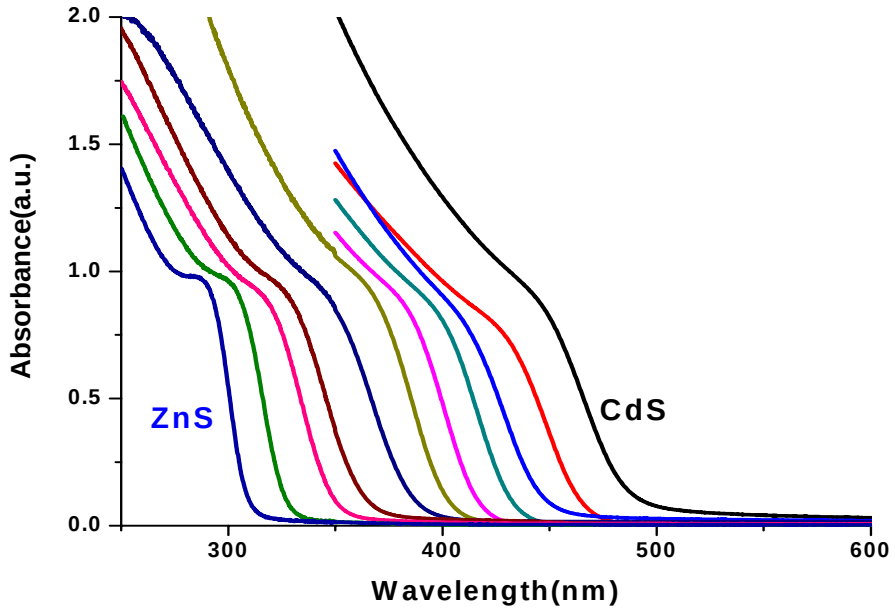

Fig.3.2.8. The UV-Vis absorption spectra of nano-$Cd_{1-x}Zn_xS$-meso-SiO_2 films, the spectra in between the spectra of CdS and ZnS are from the $Cd_{1-x}Zn_xS$ nanocrystals, where x is increasing from 0.1 to 0.9 with an increment of 0.1 going from CdS side to ZnS side).

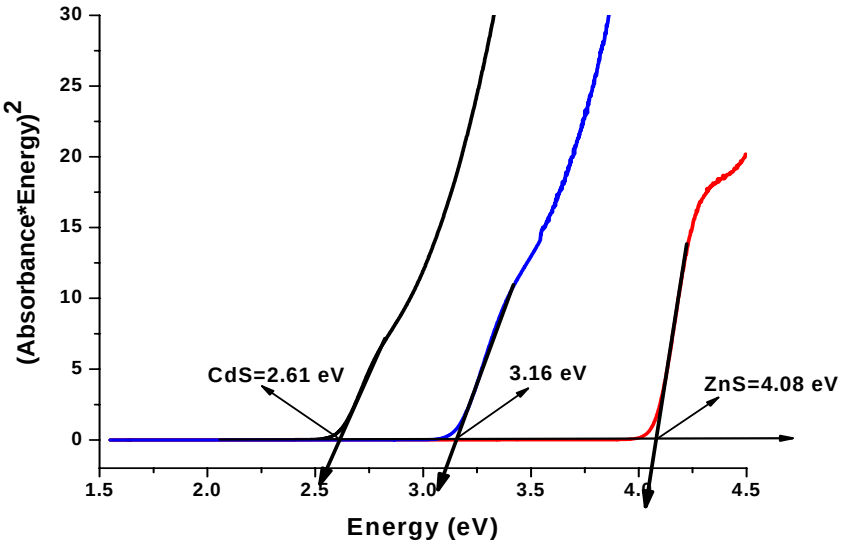

Fig.3.2.9. Band-gap values of three compositions in nano-$Cd_{1-x}Zn_xS$-meso-SiO_2 films, when x is equal to 0.0 for CdS, 0.5 for $Cd_{0.5}Zn_{0.5}S$ and 1.0 for ZnS nanoparticles.

The absorption spectra of the nanocrystalline semiconductor samples display exciton absorption bands at higher energy than absorption edges of bulk semiconductor materials. This result is a consequence of strong quantum confinement effect that is obtained by the reduced size of the nanoparticles as compared to the exciton Bohr diameter of bulk semiconductors. For example, CdS Bohr diameter is ~ 12 nm.[31] Figure 3.2.10 shows plots of the band-gap values of nano-$Cd_{1-x}Zn_xS$-meso-SiO_2 materials[132] and the bulk counterparts with composition, x.

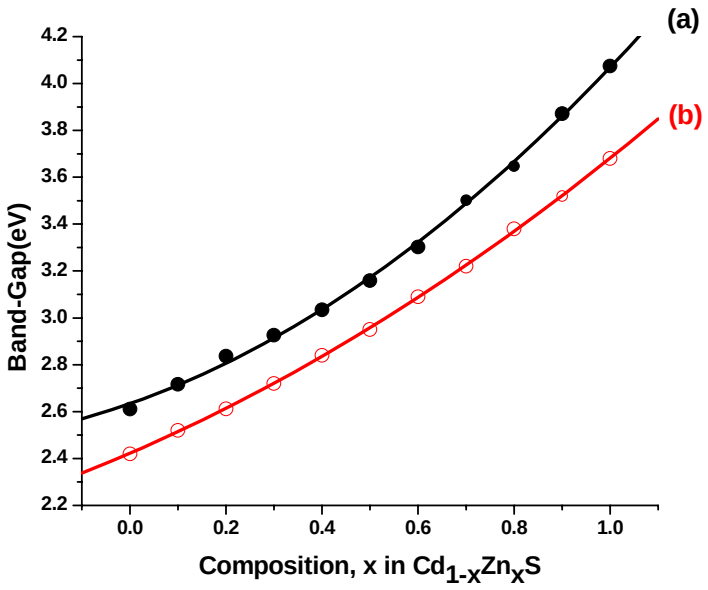

Fig. 3.2.10. Plots of E_g versus x of (a) nano-$Cd_{1-x}Zn_xS$-meso-SiO_2 and (b) bulk materials.

The blue shift from the bulk E_g values by 0.19 and 0.40 eV for the two end compositions, CdS and ZnS, respectively, indicates that the particle size is smaller in the Zn(II) rich end of the $Cd_{1-x}Zn_xS$ nanocrystals.

In a strong confinement regime like in the case of nanosized semiconductor particles, Brus[138] proposed the relationship (equation 4) between bulk band gap and nanoparticle band gap;

$$E(R) = E_g + \frac{\hbar^2}{2}\left(\frac{1}{m_e^*} + \frac{1}{m_h^*}\right)\frac{\pi^2}{R^2} - 1.786\frac{e^2}{\epsilon R} - 0.248\ E_{Ry}^* \qquad (4)$$

where E_g is the bulk band gap, R is nanocrystalline radius and it is much smaller than the Bohr exciton radius in the strong confinement regime. The second term in the formula mainly determines the band gap shift from bulk values because it inversely depends on square of R. Therefore, ZnS must have smaller radius than CdS radius.

Recently, Sarma et al.[139-140] used the tight-binding (TB) model to evaluate the electronic structure of II-VI semiconductors in real space developed for the bulk II-VI semiconductors. Equation (5) has been obtained from the sp^3d^5 TB model that uses cation-anion and anon-anion interactions in comparison with sp^3s^* and experimental data points by Sarma et al.[140] We used Sarma's expression (eq. 5) to analyze the variation in the electronic structure of nanocrystals as a function of their size and composition. This method has several advantages over Brus's model such as it provides a considerable enhancement in the accuracy of the results.

$$\Delta E_g = a_1 e^{-d/b1} + a_2 e^{-d/b2} \qquad (5)$$

The variation in the band gap difference ΔE_g between the bulk crystals and nanocrystals with the diameter (d) of the nanocrystals can be calculated from the empirical formula (5). The values of the parameters a and b used in equation 5 for all the $A^{II}B^{VI}$ semiconductors studied by tight-binding model were tabulated in Table 3.2.1.[140]

	ZnS	ZnSe	ZnTe	CdS	CdSe	CdTe
a_1	7.44	2.65	5.10	2.83	7.62	5.77
b_1	2.35	7.61	10.35	8.22	6.63	8.45
a_2	3.04	1.90	1.05	1.96	2.07	1.33
b_2	15.30	23.50	97.93	18.07	28.88	43.73

Table 3.2.1 Parameters of a and b used in equation (5) for ZnS, ZnSe, ZnTe, CdS, CdSe, and CdTe in tight-binding model.[140]

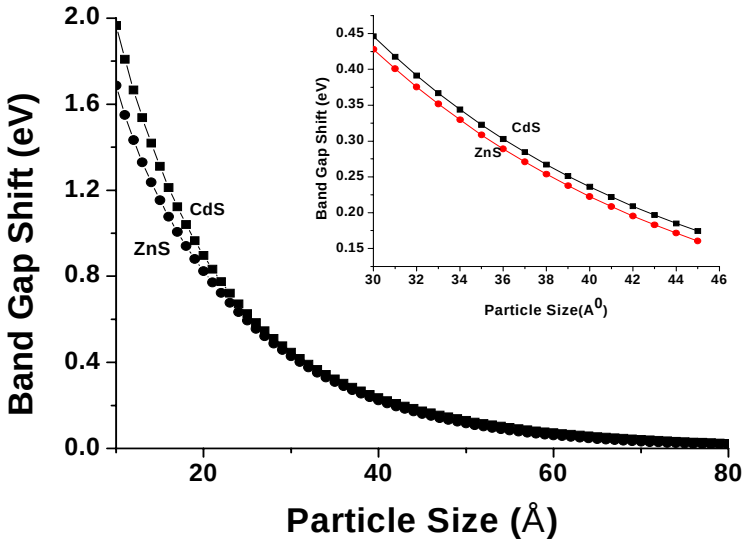

Fig. 3.2.11 Plots of band-gap shift (ΔE_g) of CdS and ZnS obtained from an empirical formula of equation (5) versus particle size (Å). The inset is the same plot showing the regions used in this work.

The equation (5) provides band gap difference between the bulk and nanosized semiconductors of ZnS, ZnSe, ZnTe, CdS, CdSe and CdTe in the diameter (d) range of 5 to 80 Å. Figure 3.2.11 shows a plot of the band gap shift versus particle size, in a range of 5 to 80 Å by using a and b parameters of CdS and ZnS in Table 3.2.1. Above 8-10 nm, the nanoparticles behave like bulk materials. The inset in Figure 3.2.11 shows the intervals between 0.1 and 0.5 eV, where all the band gap difference from our samples are located. Using the plot, we calculated the particle size of the CdS and ZnS nanoparticles as 4.4 and 3.1 nm, respectively. In the fresh samples, variation in the $Cd_{1-x}Zn_xS$ nanocrystals band gaps and particle size were evaluated using the same plot in Fig.3.2.11.

Figure 3.2.12 shows the variation in the particle size of the $Cd_{1-x}Zn_xS$ nanocrystals with x. This observation is consistent with the XRD results, in which the diffraction lines broaden and shift to higher angle going from CdS to ZnS nanocrystals. The intermediate compositions display an almost linear dependence (Vegard's type plot) on the

composition, which indicates solid-solution behavior in the nano-$Cd_{1-x}Zn_xS$-meso-SiO_2 materials. The Vegard's law explains that physical properties of a mixed compound such as band gap properties of semiconductors roughly dependent on the compositions of the component binaries.

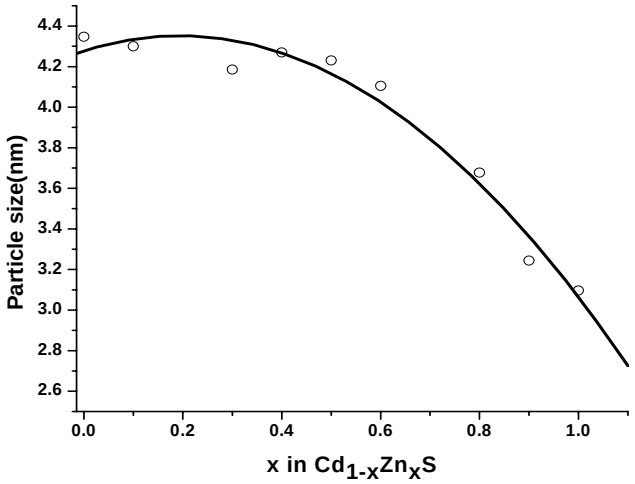

Fig. 3.2.12. A plot of particle size evaluated from Fig. 3.2.11 versus x in the nano-$Cd_{1-x}Zn_xS$-meso-SiO_2.

3.3 EFFECT OF AGEING OVER THE SIZE OF CdS, ZnS and $Cd_{1-x}Zn_xS$ NANOPARTICLES IN MESOSTRUCTURED SILICA FILMS

The thin films were aged with time at room temperature or at higher temperatures to enhance the silica polymerization and to obtain rigid silica walls that provide another control on particle size of the nanocrystallites. In the fresh samples, silica was not fully polymerized to form rigid silica walls between the channels. Notice that the sharp diffraction line of mesostructured silica at around 1.85^0, (d= 4.8 nm), 2θ, broadens and shifts to lower angle 1.58^0 (d= 5.6 nm) upon H_2S reaction. The origin of this shift and broadening is the soft nature of silica walls that expands with the growth of the $Cd_{1-x}Zn_xS$

nanoparticles in the channels. Therefore, the channel pore size increases from 4.7 nm to 5.5 nm. However, the aged samples do not respond, no shift or broadening, to the H_2S reaction, because with ageing the silica walls become rigid (strong enough) that limits the growth of the $Cd_{1-x}Zn_xS$ nanoparticles inside the channels.

Figure 3.3.1 shows resistivity of the pore walls to H_2S reaction upon ageing. Notice that the diffraction line at 1.80^0 is unaffected if the sample is aged 5 hours or longer at RT and reacted under H_2S atmosphere. The diffraction line of the aged sample, from 1 day to 3 days even shifts to a higher angle, due to further condensation of the silica walls (Condensation of SiOH groups).

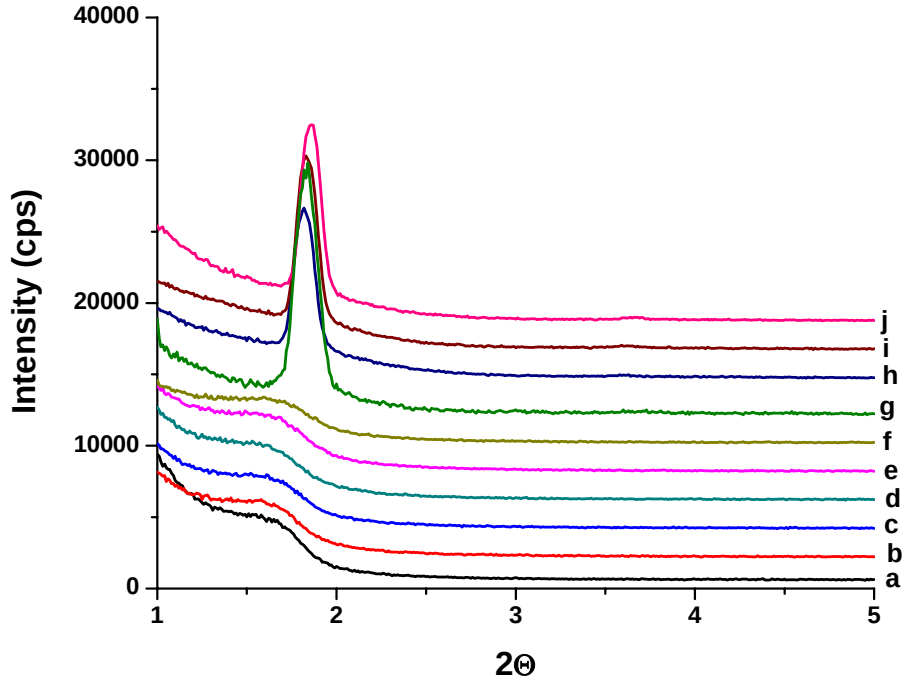

Fig.3.3.1. The XRD patterns of nano-CdS-meso-SiO_2 film samples at RT for different ageing times, a) 5 min b) 30 min c) 60 min d) 80 min e) 110 min f) 150 min g) 5 hours h)1 day i) 2days j)3 days.

Fig. 3.3.2 shows the XRD patterns of $[Zn(H_2O)_6](NO_3)$-meso-SiO_2 and nano-ZnS-meso-SiO_2 films. Notice that the 1 hour and 4 hours aged samples were not fully polymerized and gave response to H_2S reaction, but upon ageing for 1 and 2 days gave rigid silica walls. Therefore, diffraction line was unaffected in the aged samples upon H_2S reaction. The mixed salt containing silica materials also have a similar behaviour. The 1-hour and 4 hours aged samples show enlargement of the pores, however, the pore size slightly decreases in 1 day and 2 days aged samples upon H_2S reaction, Figure 3.3.3.

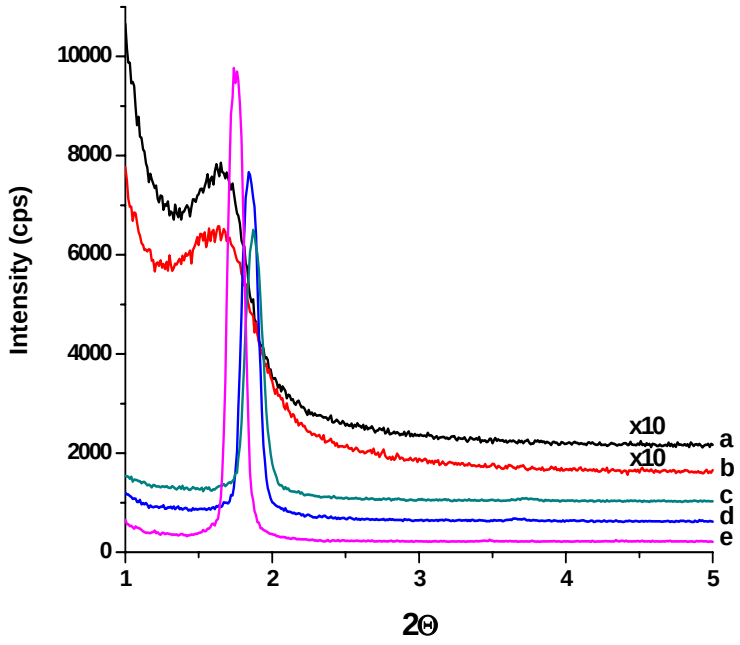

Fig.3.3.2. The XRD patterns of $[Zn(H_2O)_6](NO_3)_2$-meso-SiO_2 and nano-ZnS-meso-SiO_2, nano-ZnS-meso-SiO_2 after ageing at RT for a) 1 hour, b) 4 hours, c) 1 day, d) 2 days e) before H_2S reaction.

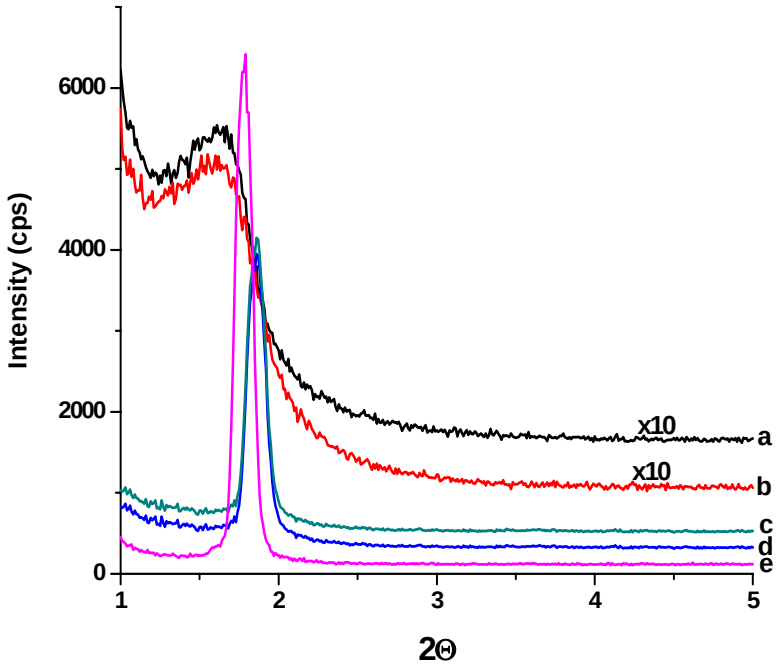

Fig.3.3.3. The XRD patterns of nano-$Cd_{0.5}Zn_{0.5}S$-meso-SiO_2 aged at RT before H_2S reaction for a) 1 hour, b) 4 hours, c) 1 day, d) 2 days and e) $([Cd(H_2O)_4](NO_3)_2)_{0.5}$-$([Zn(H_2O)_6](NO_3)_2)_{0.5}$-meso-$SiO_2$ before H_2S reaction

Effect of ageing over the size of CdS nanoparticles in mesostructured silica was also investigated using UV-Visible spectroscopy. Fig. 3.3.4. displays absorption edges of the thin film samples nano-CdS-meso-SiO_2 (aged at RT for 30 minutes, 3 hours, 5 hours, 1 day and 2 days periods and before H_2S reaction). The absorption edge blue shift with ageing. In the fresh samples, for example, 1-day aged at RT, the absorption edge appears at around 495 nm and is relatively broad. However, aged samples display sharper absorption edges. Therefore, the nanoparticles obtained from the fresh samples are larger than aged samples and have relatively broader size distributions.

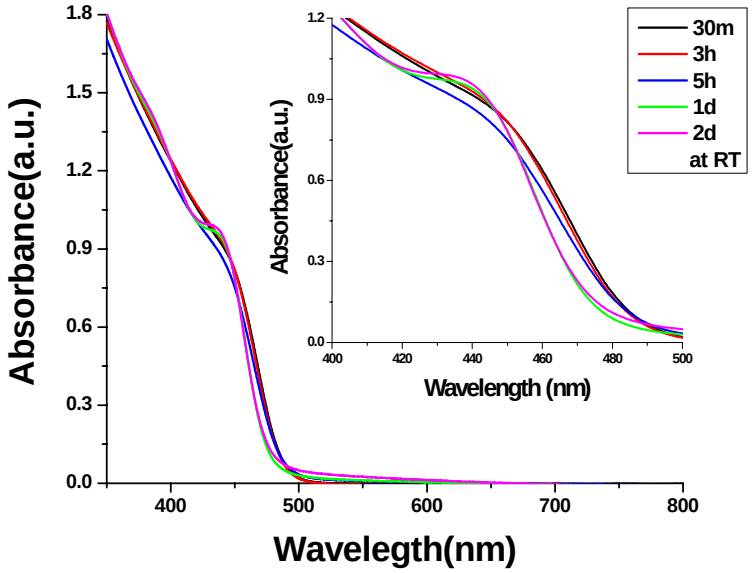

Fig.3.3.4. The UV-Vis absorption spectra of nano-CdS-meso-SiO_2 films, after ageing 30min, 3hours, 5hours, 1day and 2 days. The inset is the same graph showing the regions of absorbance variation clearly.

The rigidity of the silica walls increases with heating so the growth of nanoparticles inside the channels was further confined. Figure 3.3.5 shows the XRD patterns of nano-CdS-meso-SiO_2 and $[Cd(H_2O)_4](NO_3)_2$-meso-SiO_2 samples that were aged at 100^0C for 30 minutes and 3 days before the H_2S reaction. The diffraction patterns of the samples are the same for both conditions, because the rigid silica walls restrict the growth of the nanoparticle.

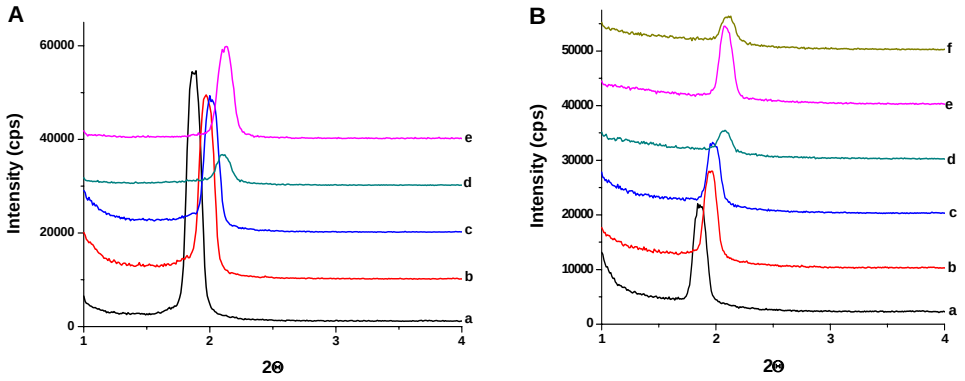

Fig.3.3.5. The XRD patterns of $[Cd(H_2O)_4](NO_3)_2$-meso-SiO_2 and nano-CdS-meso-SiO_2, **(A)** $[Cd(H_2O)_4](NO_3)_2$-meso-SiO_2 pre-reaction after aging at 100^0C a) 30 min b) 3 hours, c) 5 hours, d) 1 day e) 2 days. **(B)** nano-CdS-meso-SiO_2 after aging at 100^0C a) 30 min b) 3 hours, c) 5 hours, d) 1 day e) 2 days f) 3 days.

In order to analyze the temperature effect on the aging process, Figure 3.3.6 compares the film samples that were aged at RT and 100^0C for 30 minutes, 5 hours, and 2 days and then reacted with H_2S. The growth of CdS nanoparticles inside the channels enlarged the pores in the sample that was only aged at RT for 30 minutes. However, the samples aged at 100^0C for 30 minutes and at RT for 5 hours, silica condensation were enough to limit the nanoparticle growth.

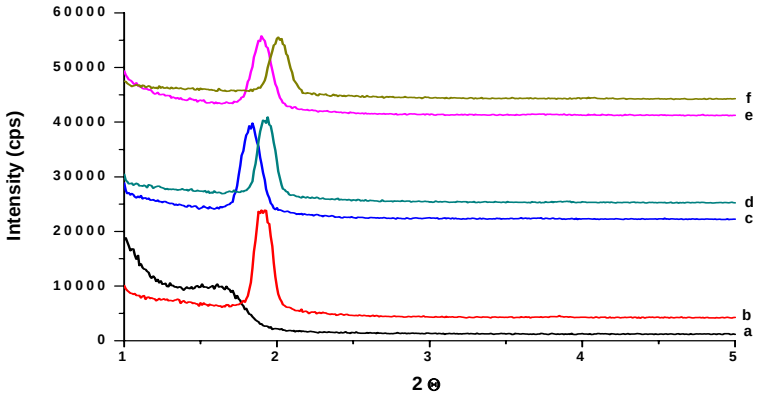

Fig.3.3.6. Comparison of nano-CdS-meso-SiO_2 XRD patterns aged at RT and 100^0 C before H_2S reaction, a)30 min, RT b) 30 min, 100^0C , c)5 hours, RT d) 5 hours, 100^0C e) 2 days, RT f) 2 days, 100^0C.

The silica condensation constantly shrinks the silica walls until it collapses at high temperatures. Figure 3.3.7 (A) and 3.3.7 (B) respectively show the XRD patterns of the film samples before and after H_2S reactions. The film samples are stable up to 240^0C and the particles formed in the film samples aged at 240^0C have more uniform size distribution.

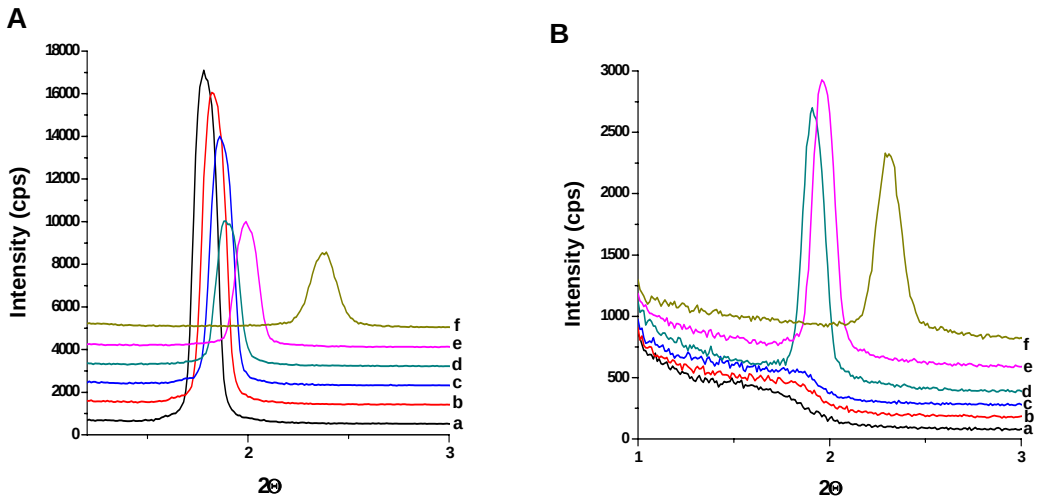

Fig. 3.3.7. The XRD patterns of $[Cd(H_2O)_4](NO_3)_2$-meso-SiO_2 and nano-CdS-meso-SiO_2 **(A)** $[Cd(H_2O)_4](NO_3)_2$-meso-SiO_2 pre-reaction after ageing at a) RT, b) 50^0C, c)100^0C, d)150^0C, e) 200^0C, and f) 240^0C. **(B)** nano-CdS-meso-SiO_2 after ageing at a) RT, b) 50^0C, c)100^0C, d)150^0C, e) 200^0C, and f) 240^0C.

A comparison between the aged (at various temperature) and fresh samples has been displayed in Fig.3.3.8, using UV-Vis electronic absorption spectroscopy. The sample aged at 50^0 C has absorption edge that starts at 490 nm, whereas the sample aged at 240^0 C has an absorption edge at 465 nm. Moreover, the absorption edges of the aged samples are relatively sharper, also indicating uniform nanoparticle size distribution (200-240^0 C).

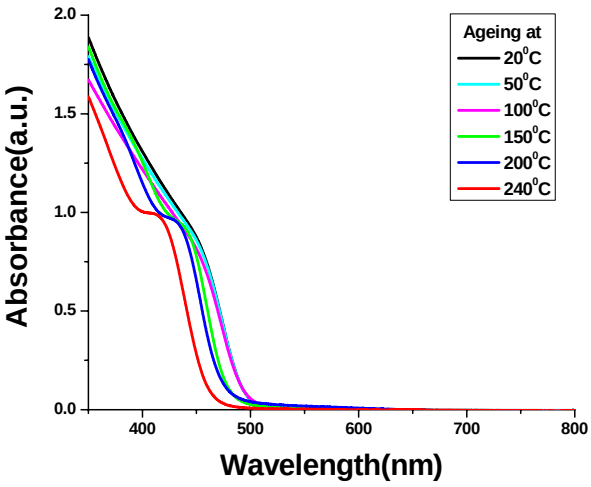

Fig. 3.3.8. The UV-Vis absorption spectra of nano-CdS-meso-SiO_2 films, after ageing at 20^0 C, 50^0 C, 100^0 C, 150^0 C, 200^0 C, 240^0 C with a time interval of 45 minutes.

The band-gap values of the CdS nanoparticles in the fresh and aged thin films with temperatures were evaluated to be between 2.6 eV and 2.8 eV. Figure 3.3.9 shows the absorption spectra of nano-CdS-meso-SiO_2 that display a blue shift going from 20^0C to 240^0C. This trend indicates that the nanoparticles are smaller in the samples aged at higher temperatures.

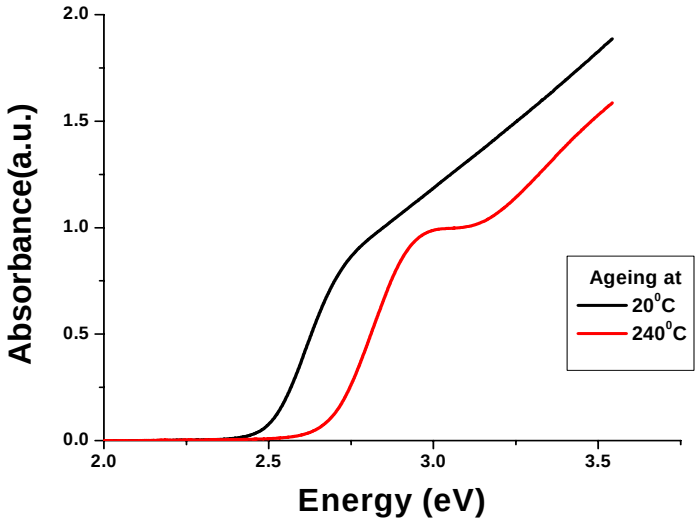

Fig. 3.3.9. The UV-Vis spectra of nano-CdS-meso-SiO_2 thin films aged at 20^0C and 240^0C.

The surfactant molecules can be removed from the silica channels by washing the films after the H_2S reaction with 1:1 (v:v) ethanol/water solution.[49] During the H_2S reaction, especially in the thicker samples, many $SiOH_2^+$ acid sites that slowly attack to nanoparticles to decompose them into ions. These samples loose their colors in time and are smelly. However, washing the samples removes the acid in the channels and stabilizes the nanocrystallites. Washing does not disturb the structure of nanoparticles and mesostructured silica host. Therefore, the washed samples still diffract at low and high angles, due to mesostructure and nanocrystallites, respectively. However, washing the film samples causes further shrinking on the silica pores, because part of the surfactant molecules are removed from the channels. Figure 3.3.10 shows the XRD patterns of the CdS-meso-SiO_2 films that have been aged at 150^0C and 220^0C and then washed with ethanol-water mixture shrink considerably. The shrink is from 3.7 nm to 3.0 nm by washing after H_2S reaction (Fig. 3.3.10 e, f respectively)

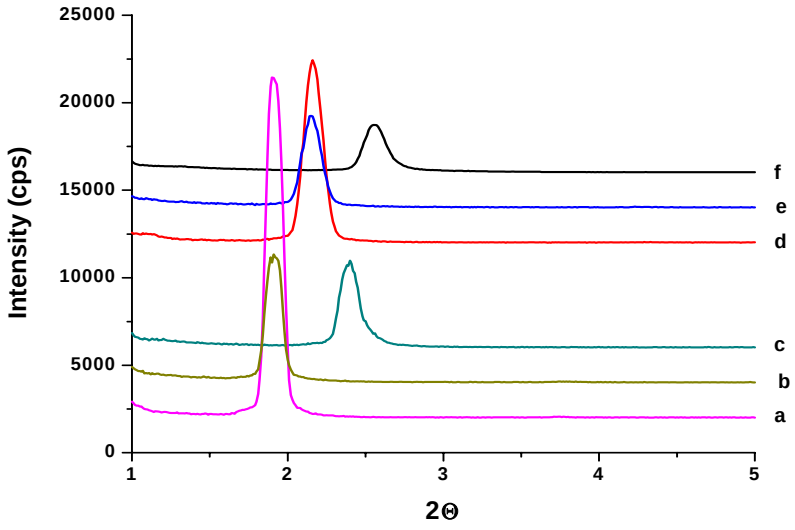

Fig.3.3.10. The XRD patterns of films that are; a) $[Cd(H_2O)_4](NO_3)_2$-meso-SiO_2 aged at 150^0C, b) nano-CdS-meso-SiO_2, aged at 150^0C c) nano-CdS-meso-SiO_2, aged at 150^0C and washed with 1:1 ethanol-water mixture, d) $[Cd(H_2O)_4](NO_3)_2$-meso-SiO_2 aged at 220^0C, b) nano-CdS-meso-SiO_2, aged at 220^0C c) nano-CdS-meso-SiO_2, aged at 220^0C and washed with ethanol-water mixture.

The pore size gradually decreases with increasing ageing temperature. 250^0C is the maximum temperature to get the smallest silica channels in our system. Above this temperature, the mesostructure collapses and the diffraction line at low angle disappears (except calcination process). Figure 3.3.11 shows the XRD patterns of $[Cd(H_2O)_4](NO_3)_2$-meso-SiO_2, aged at 250^0C and treated at RT under H_2S atmosphere. Note that the ageing process were carried by increasing the temperature from RT to 250^0C in 1 hour and kept at 250^0C for 20 minutes. The sample treated at 250^0C had a diffraction line at 2.88^0 (Fig. 3.3.11 a) before H_2S reaction. It shifts to 3.28^0, 2θ, after the H_2S reaction and washing with ethanol-water (1:1, v:v) mixture. This is the maximum shrinking case in our system in which the pore diameter has reached to minimum value, 2.1 nm, (Diffraction at 3.28^0, and d= 2.7 nm.), Fig 3.3.11 b.

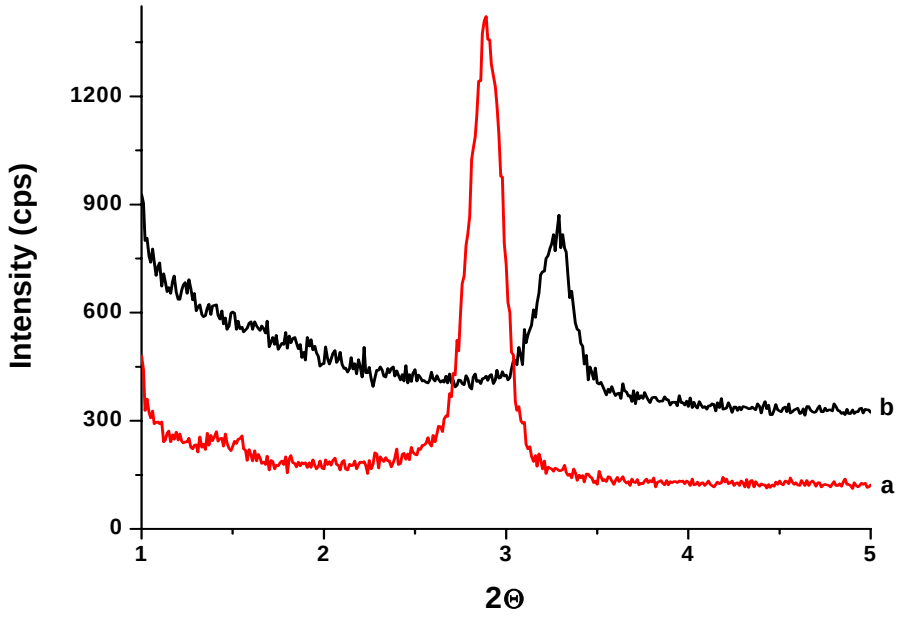

Fig.3.3.11. The XRD patterns of films that are a) before reaction, $[Cd(H_2O)_4](NO_3)_2$-meso-SiO_2 aged at 250^0C, b) after reaction, nano-CdS-meso-SiO_2, aged at 250^0C and washed with ethanol-water solution.

Therefore, the size of the nanocrystallites can be controlled by controlling the ageing temperature of the silica films and washing the film samples with ethanol-water mixture. The pore size can be changed between 4.7 nm to 2.1 nm. This influences the growth process of the metal sulfides, such that more uniform size distributions of the nanocrystallites can be obtained from the aged samples. However, ageing usually creates other problems, like cracks on the films, collapse of the pores at higher temperatures etc. The optimum conditions in our system seems to be, ageing in between RT (longer time) and 240^0C.

3.4 THERMAL PROPERTIES OF NANOCRYSTALLS

The thermal properties of the nanocrystallites were also investigated by heating the nano-$Cd_{1-x}Zn_xS$-meso-SiO_2 samples at different temperatures. The structure of the film samples is stable before the reaction until at 250^0C. After the reaction, heating the samples further shifts the diffraction line to higher angles. Figure 3.4.1 shows diffraction patterns recorded at various stages of heating of the nano-$Cd_{1-x}Zn_xS$-meso-SiO_2 film samples. Figure 3.4.1 (A) shows the changes on the fresh sample after reaction under H_2S and then heated at higher temperatures (RT to 250^0C). The structure becomes disordered at around 250^0C. It is also the same in the aged samples, the silica channels became disordered at high temperature treatments and the nanoparticles inside the silica channels decomposed.

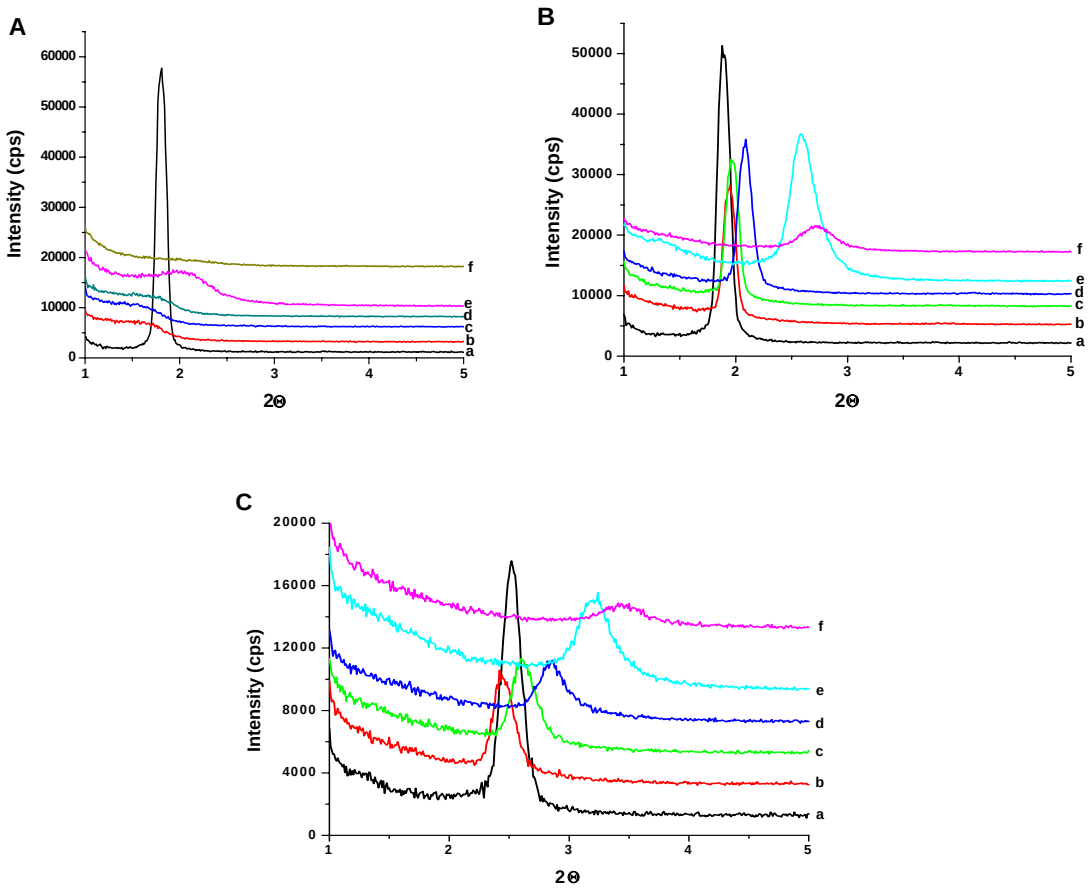

Fig. 3.4.1. The XRD patterns of nano-CdS-meso-SiO_2 samples, a) before reaction, b) after reaction, and heating after reaction at c) 75^0C, d) 150^0C, e) 250^0C f) 250^0 C for 5 hours. **A)** No ageing before the reaction, **B)** Aged at 150^0C before the reaction, and **C)** Aged at 240^0C before the reaction.

The thermal behaviour of nano-$Cd_{1-x}Zn_xS$-meso-SiO_2 materials were also followed using UV-Vis absorption method. Fig. 3.4.2 shows the variation of the absorption spectra of fresh and aged samples at various temperatures. After H_2S reaction, a sharp absorption edge appears that remains up to 150^0C. However, above 150^0C, the absorption edge broadened and blue shifted. It means that the CdS nanoparticles started to decompose

above 150^{0}C. Further heating (up to 450^{0}C) removes the surfactant molecules and oxidize CdS particles to CdO particles (see next section).

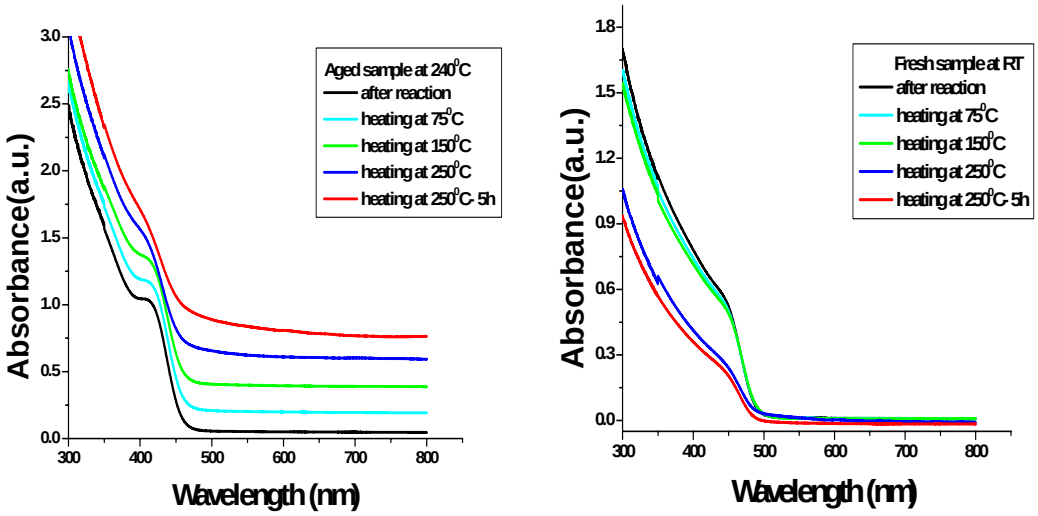

Fig. 3.4.2. The UV-Vis spectra of heated nano-CdS-meso-SiO_2 at different temperatures.

3.5. CALCINATION PROCESS

High temperature calcination (~450°C) is the most commonly employed procedure for removing the organic surfactant molecules while maintaining the initial structure of the silica. Another method that allows the removal of the surfactant is solvent extraction. Both methods were used to extract the organic surfactant molecules from the thin films. Fig. 3.3.10 shows that the pore size of the silica channels was reduced by washing the samples with ethanol/water solution (because of removing surfactant molecules). However, when high temperature calcination was applied, the pore size of the silica channels decreased more than the solvent extraction method. The reason is further silica condensation during the heating process.

In case of washing the samples, the decrease in pore size is 1.0 nm, from 4.3 nm to 3.3 nm, see Fig 3.3.10 b, c. However, calcination at 450^0C causes 1.6 nm shrinkage from 4.3 nm to 2.7 nm, Figure 3.5.1. Therefore, the silica polymerization is a very important step for controlling the channels dimensions. Fig 3.4.1 (B) displayed XRD patterns of the samples after heating at high temperatures. The pore size decreased by 1.5 nm from 4.2 nm to 2.7 nm (Fig.3.4.1 B- b, f) at 250^0C. This degree of condensation seems very close to calcination value. These results are summarized in Table 3.5.1.

Applied Methods by	d-spacing(nm) (pore size)	Final d-spacing (nm) (pore size)	Size difference(nm)
washing	4.6 (4.3)	3.7 (3.3)	1.0
heating (250^0C)	4.5 (4.2)	3.2 (2.7)	1.5
calcination (450^0C)	4.6 (4.3)	3.2 (2.7)	1.6

Table.3.5.1 Silica channels size difference after applying three methods.

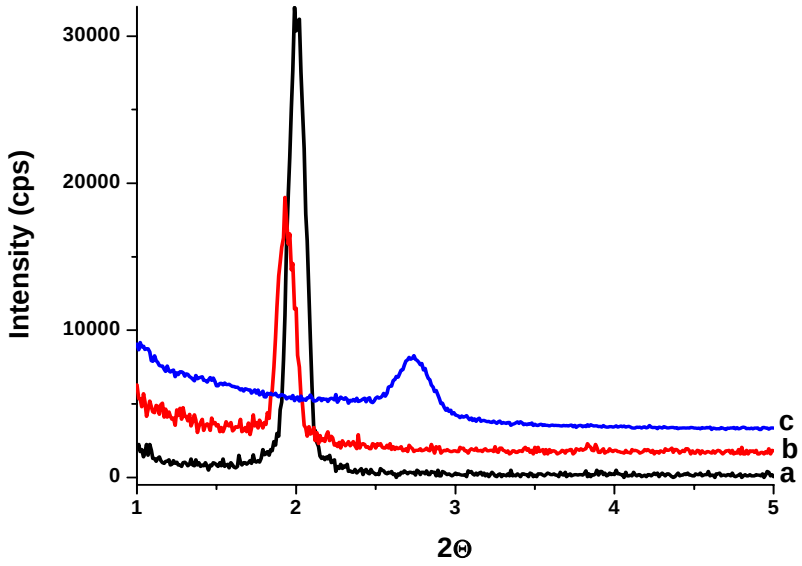

Fig. 3.5.1. The XRD patterns of the nano-CdS-meso-SiO_2 samples that was aged at 170^0C, a) before reaction, b) after reaction, and c) calcination after reaction at 450^0C (the temperature was gradually increased in 5 hours from RT to 450^0C and heated for 5 hours at 450^0C)

The high temperature (~ 450^0C) calcination is not the best way to remove the organic surfactant molecules, because the semiconductor $Cd_{1-x}Zn_xS$ nanoparticles oxidize in the channels of the film samples at these temperatures. However, the calcined samples can be reacted above 150^0C under H_2S atmosphere to reform the nanoparticles inside the empty silica channels. Fig. 3.5.2 shows UV-Vis absorption spectra of the nano-CdS-meso-SiO_2 samples calcination at 450^0 C. The absorption edge of CdS nanoparticles starts at 495 nm, Figure 3.2.8. However, after calcination, under air, the absorption edge of CdS disappeared and another strong absorption edge appeared at around 267 nm. At high temperatures, the CdS nanoparticles convert to CdO nanoparticles. However, CdO can be reacted under H_2S atmosphere at 150^0C to regenerate the CdS nanoparticles in the silica channels. The color of the film samples is yellow before calcination. However it becomes colorless upon calcination at 450^0C. The color of the powder samples calcined at 450^0C turns to yellow upon H_2S reaction at 150^0C indicating the regeneration of CdS

particles. However, it is difficult to measure the absorption spectrum of this sample in transmittance mode due to presence of many cracks on the film samples.

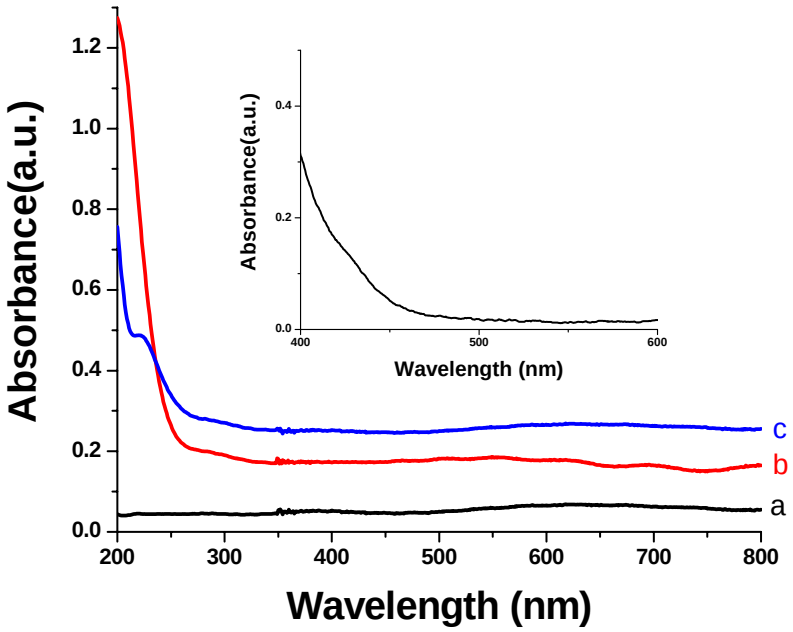

Fig. 3.5.2. The UV-Vis absorption spectra of calcined films at 450^0C that was aged at 170^0C, a) salt free system, b) before H_2S reaction, and c) nano-CdS-meso-SiO_2. The inset is the sample c but reacted with H_2S at 150^0C

FT-IR spectroscopy also provides information about the calcination process. Figure 3.5.3 compares the FT-IR spectra before and after the calcination. The surfactant related methylene symmetric and anti-symmetric vibrations, at 2854 and 2923 cm^{-1} respectively, CH_2 rocking modes at 1465 and 1351 cm^{-1} and CH_2 twisting vibrations at 1297 cm^{-1} disappeared upon calcination. The Si-O antisymmetric stretching that has an intense band around 1000-1300 cm^{-1} and Si-O symmetric stretching at 800 cm^{-1} did not alter. In addition, Si-O stretching modes of silanol (Si-OH) band at 953 cm^{-1} disappeared. It shows that silanol groups have further condensed at high temperatures.

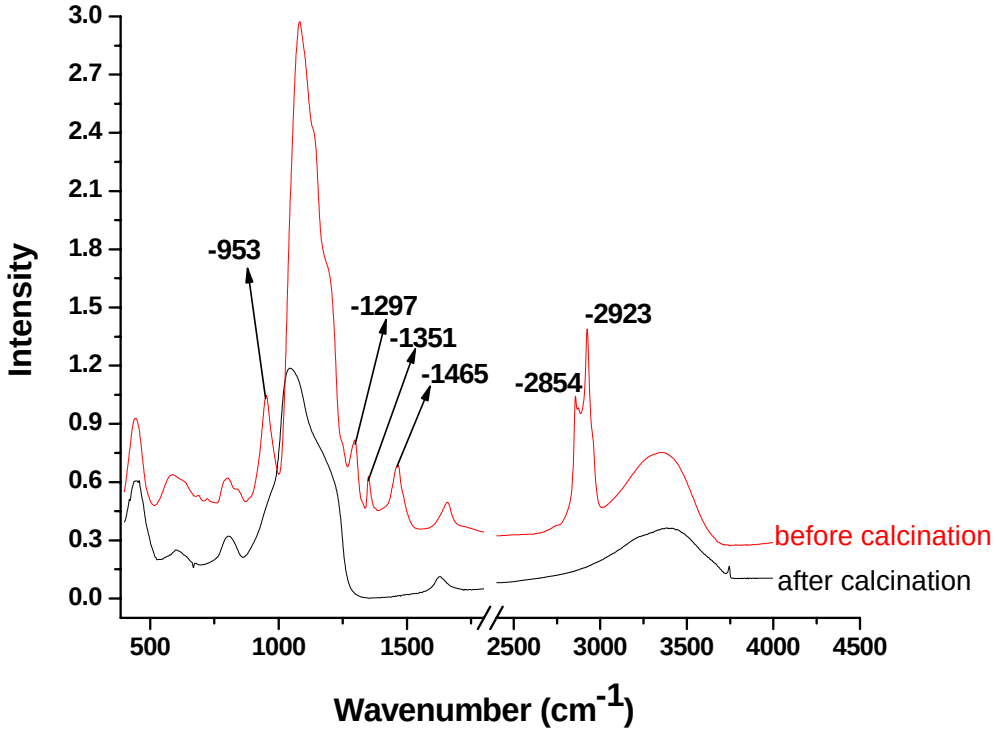

Fig. 3.5.3. The FT-IR spectra of nano-CdS-meso-SiO_2 before and after calcination at 450^0C.

3.6. Future Work

This work can be extended to Pluronic systems. The transition metal salts (TMS) also dissolves in tri-block co-polymers, Pluronics (L64, P65 and P123) also form LC mesophases in the presence and absence of free water in the media.[91,141] The Pluronics, $(PEO)_x(PPO)_y(PEO)_x$, PEO= - CH_2 CH_2O- and PPO = -$CH(CH_3)$ CH_2O-, can be used as templating agents for the synthesis of nanoparticles, like oligo ethylene oxide type surfactants. The most commonly used Pluronic is P123, where x is 20 and y is 70 on average. The P123 produces mesoporous materials with larger pores, thicker walls. Different types of structures could be produced in the H_2O:TMS:P123 systems, such as

lamella, cubic and tetragonal with salt:P123 mole ratio of 6, 7, and 4, respectively.[91] Silica addition to the system provides rigidity and preserves the structure of LC mesophase in solid phase.

A mixture of TMOS, water, acid, and surfactant (P123) with a composition of 1.6 g: 3.0 g: 0.1 g: 1.0 g, respectively and 3.0 mole ratio of salt:surfactant produce lamellar mesostructured silica materials. Figure 3.6.1 (A) shows XRD patterns of $[Cd(H_2O)_4](NO_3)_2$-meso-SiO_2. The lines at 98.1, 49.6, 33.3, 25.1 Å d-spacing values, corresponding to (001), (002), (003), (004) lines, respectively, of a lamella mesophase with unit cell parameter c=99.1 Å. Figure 3.6.1 (B) shows electronic absorption spectrum of the CdS nanoparticles produced between the lamella layers. The absorption edge in the P123 system is blue shifted with respect to $C_{12}EO_{10}$ system; however, the CdS size distribution is not as uniform.

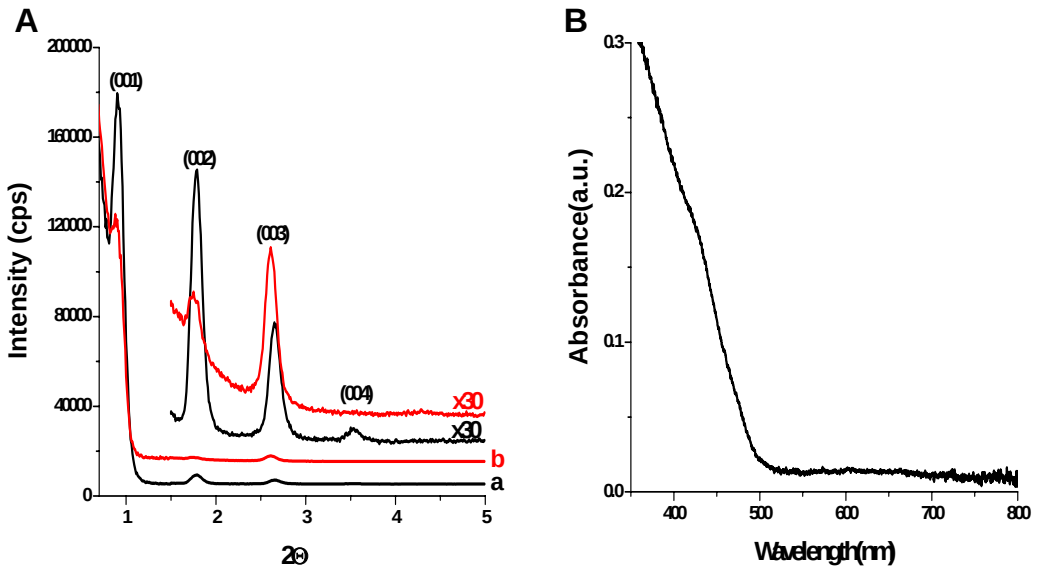

Fig. 3.6.1. (A) The XRD patterns of a)$[Cd(H_2O)_4](NO_3)_2$-meso-SiO_2 and b)nano-CdS-meso-SiO_2 and (B) The UV-Vis spectrum of nano-CdS-meso-SiO_2 with $[Cd(H_2O)_4](NO_3)_2$:P123 mole ratio of 3.0.

P123 surfactant molecule has a very large molecular weight (M_{av}= 5800) so it can accommodate more salt ions than C_nEO_m surfactants. The salt:surfactant ratio can be increased up to a 15 mole ratio.[91] In the optimum conditions, P123 could provide rich structures to synthesize nanoparticles with various dimensions and structures. Therefore, P123 can be used in our system to obtain $Cd_{1-x}Zn_xS$ nanoparticles. Notice that the structure of the fresh silica host did not alter upon H_2S reaction indicating that the silica walls are relatively resistive to CdS growth. Further studies are required to elucidate the details of P123-silica systems.

4. Conclusion

In this thesis, a new and simple method has been developed to synthesize $Cd_{1-x}Zn_xS$ nanocrystals in the channels of mesostructured silica. In the nanocrystals, the composition can be changed from x = 0.0 to 1.0. The initial salt amounts of Cd(II) and Zn(II) ions determines the final composition of nanocrystals. The nanocrystallites can be homogeneously distributed into the channels of mesostructured silica thin films by combining the LCT approach and MLC mesophase. The silica polymerization process affects the channels' dimensions, such that the fresh samples have larger pores than aged samples. These film samples can be reacted under H_2S gas to produce a solid-solution of nanocrystalline $Cd_{1-x}Zn_xS$ in the channels of mesostructured silica films. Their band gaps display a blue shift from the bulk values and also going from CdS to ZnS. The optical band-gaps of the $Cd_{1-x}Zn_xS$ nanocrystals are in between 2.6 eV and 4.1 eV for two end compositions, CdS and ZnS, respectively. The particle growth and size distribution inside the silica channels are strongly influenced by ageing the film samples. Aged samples have rigid silica walls that limit the nanoparticle growth, however fresh samples are not fully polymerized and give response to H_2S reaction. The band gap value also show response, to ageing, a blue shift and sharper absorption-edges. Therefore, aged samples have more uniform size distribution and smaller nanoparticles.

The nano-CdS-meso-SiO_2 samples decompose at higher temperatures above 250^0C and the fast heating collapses the mesostructure. However, calcination process (slow heating) preserves the structure of the silica host up to 450^0C. The silica walls shrink and the CdS particles transform to CdO, metal oxides, at higher temperatures. However, H_2S reaction regenerates CdS particles inside the silica channels. The P123 surfactant can also be used to synthesize $Cd_{1-x}Zn_xS$ nanocrystals in relatively larger space. It provides rich structures and stability to the synthesis of metal sulfide nanoparticles in different host structures.

The method developed in this thesis is very flexible to synthesis of metal sulfides and mixed metal sulfides with relatively uniform size distribution. The method can be extended to other metal ion systems, such as Mn (II), Co (II), Ni (II) etc. and metal selenides.

5. REFERENCES

[1] P. J. Collings, M. Hired, Introduction to Liquid Crystals, Taylor&Francis, 1997.

[2] J. Collings, Liquid Crystals, Princeton University Press, 1990.

[3] T. M. Dellinger, P. V. Braun, *Chem. Mater.* **16**, *2201*,2004.

[4] B.A. Korgel, H.G. Monbouquette, *J. Phys. Chem*. **100**, *346*, 1996.

[5] M. Pileni, B.W. Ninham, J. Tanori, I. Lisievcki, A. Filankembo, *Adv. Mater*. **11**, *1358*, 1999.

[6] S. Mann, S. Burkett, S. A. Davis, *Chem. Mater*. **9**, *2300*, 1997.

[7] G. Soler-Illia, E. Crepaldi, D. Grosso, C. Sanchez, *Current Opinion in Colloid and Interface Science* **8**, *109*, 2003.

[8] IUPAC Manual of Symbols and Terminology, Appendix 2, Part 1, *Colloid and Surface Chemsitry* **31**, *578*, 1972.

[9] J. S. Beck, J. C. Vartulli, W .J. Roth, M. E. Leonowicz, C. T. Kresge, K. D. Schmitt, *J. Am. Chem. Soc,***114,** *10834*, 1992.

[10] T. Yanagisawa, T. Shimizu, C. Kato, *Bull. Chem. Soc. Jpn*. **63**, *988*, 1990.

[11] C. T. Kresge, M. E. Leonowicz, J. C. Vartuli, J. S. Beck, *Nature* **359**, *710*, 1992.

[12] J. Y. Ying, C. P. Mehnet, M. S. Wong, *Angew .Chem. Int. Ed. Engl*. **38**, *56*, 1999.

[13] D. Y. Zhao, J. L. Feng, Q. S. Huo, N. Melosh, G. H. Fredrickson, B. F. Chmelka, G. D. Stucky, *Science **279***, *548*, 1998.

[14] P. Schmidt-Winkel, W. W. Lukens, D. Y. Zhao, P. D. Yang, B. F. Chmelka, G. D. Stucky, *J. Am. Chem. Soc.* **121**, *254*, 1999.

[15] P. D. Yang, D. Y. Zhao, B. F. Chmelka, G. D. Stucky, *Nature* **396**, *152*, 1998.

[16] U. Ciesla, D. Demuth, R. Leon, P. Petroff, G. Stucky, K. Unger, F. Schuth, *J. Chem. Soc.* Chem. Comm. *1387*, 1994.

[17] U. Ciesla, S. Schacht, G. D. Stucky, K. K. Unger, F. Schuth, *Angew. Chem. Int. Ed. Engl*. **35**, *541*, 1996.

[18] D. M. Antonelli, A. Nakahira, J. Y. Ying, *Inorg. Chem.* **35**, *3126*, 1996.

[19] D. M Antonelli, J. Y. Ying, *Angew. Chem. Int. Ed. Engl*. **35**, *426*, 1996.

[20] M. J. MacLachlan, N. Coombs, G. A. Ozin, *Nature* **397**,*681*,1999.

[21] M. J. MacLachlan, N. Coombs, R. L. Bedard, S. White, L. K. Thompson, G.A.Ozin, *J. Am. Chem. Soc*.**121**, *12005*, 1999.

[22] P. V. Braun, P.Osenar, S. I. Stupp, *Nature* **380**, *325*, 1996.

[23] P. V. Braun, P. Osenar, V. Tohver, S. B. Kennedy, S.I. Stupp, *J. Am. Chem. Soc*. **121**, *7302*, 1999.

[24] K. K. Rangan, S. J. L. Billinge, V. Petkov, J. Heising, M. G. Kanatzidis, *Chem. Mater*. **11**, *2629*, 1999.

[25] J. Q. Li, L. F. Nazar, *Chem. Comm. 1749*, 2000.

[26] B. J. Melde, B. T. Holland, A. Stein, *Chem. Mater.* **11**, *3302*, 1999.

[27] C. Yoshina-Ishii, T. Asefa, N. Coombs, M. J. MacLachlan, G. A. Ozin, *Chem. Comm*. *2539*, 1999.

[28] S. Inagaki, S. Guan, Y.Fukushima, T. Ohsuna, O. Terasaki, *J. Am. Chem. Soc*. **121,** *9611*, 1999.

[29] Y. F. Lu, H. Y. Fan, N. Doke, D. A. Loy, R. A. Assink, D. A. LaVan, C. J. Brinker, *J. Am. Chem. Soc*. **122**, *5258*, 2000.

[30] C. Flytzanis, F. Hache, M. C. Klein, D. Ricard, P. Roussignol, *Progress in Optics* **24**, *321*, 1991.

[31] A. P. Alivisatos, *J. Phys. Chem*. **100**, *13226,* 1996.

[32] A.Y.Stakheev, L. M. Kustov, *Applied Catal. A* **188**, *3*,1999.

[33] L. L. Beecroft, C. K. Ober, *Chem. Mater.* **9**, *1302*, 1997.

[34] K.Akamatsu, S. Deki, *Nanostruct. Mater.* **8**, *1121*, 1997.

[35] N. E. Fernandes, S. M. Fisher, J. C. Poshusta, D. G. Vlachos, M. Tsapatsis, J.J. Watkins, *Chem. Mater*. **13**, *2023*, 2001.

[36] Y. D.Yin, X. L. Xu, C. J. Xia, Z. C. Zhang, *Chem. Comm. 941*, 1998.

[37] L., Schmid, O. Krocher, R. A . Koppel, A. Baiker, *Microporous Mesoporous Mater.* **35**, *181*, 2000.

[38] M. Kawashita, S. Tsuneyama, F. Miyaji, T. Kokubo, H. Kozuka, K. Yamamoto, *Biomaterials* **21**, *393*, 2000.

[39] J. Ramos, A. Millan, F. Palacio, *Polymer* **41**, *8461*, 2000.

[40] C. Castro, J. Ramos, A. Millan, J. Gonzalez-Calbet, *Chem. Mater.* **12**, *3681*, 2000.

[41] L. Wang, M. Rocci-Lane, P. Brazis, C. R. Kannewurf, Y. I .Kim,

W. Lee, J H.Choy, M.G. Kanatzidis, *J. Am. Chem. Soc*. **122**, *6629*, 2000.

[42] C.J. Brinker, K.D. Keefer, D.W. Schaffer, R.A. Assink, B.D. Kay C.S. Ashley, *J. Non-Cryst. Solids* **63**, *45*, 1984.

[43] W. H. Zhang, J. L. Shi, H. R. Chen, D.S. Yan, *Chem. Mater*. **13**, *648*, 2001.

[44] Ö.Dağ, G. A. Ozin, H. Yang, C. Reber, G. Bussiere, *Adv. Mater*. **6**, *474*, 1999.

[45] T. Hirai, H. Okuba, I. Komasawa, *J. Phys. Chem. B* **103**, *4228*, 1999.

[46] S.Besson, T. Gacoin, C. Ricolleau, J. P. Boilot, *Nano Let.* **2**, *409*, 2002.

[47] K. S. Morley, P. C. Marr, P. B, Webb, A.R. Berry, F. J. Allison, G. Moldovan, *J. Mater. Chem*. **12,** *1898,* 2002.

[48] G. S. Attard, J. C. Glyde, C. G. Goltner, *Nature* **378**, *366*, 1995.

[49] C. Tura, N. Coombs, Ö. Dağ, *Chem. Mater.* **17**, *573*, 2005.

[50] J. Fan, C. Yu, F. Gao, J. Lei, B. Tain, L. Wang, Q. Luo, B. Tu, W. Zhou, D. Zhaoe, *Angew. Chem. Int. Ed.* **42**, *3146*, 2003.

[51] Ö. Dağ, O. Samarskaya, N. Coombs, G. A. Ozin, *J. Mater. Chem*. **13**, *328*, 2003.

[52] C. Y. Lai, B. G. Trewyn, D. M. Jeftinija, K. Jeftinija, S. Xu, S. Jeftinija, V. S. Y. Lin, *J. Am. Chem. Soc*. **125,** *4451,* 2003.

[53] B. J. Scott, G. Wirnsberger, G. D. Stucky, *Chem. Mater.* **13**, *3140*, 2001.

[54] B. J. Scott, G. Wirnsberger, G. D. Stucky, *Adv. Mater*. **13**, *1231,* 2001.

[55] S. A. Johnson, D. Khushalani, N. Coombs, T. E. Mallouk, G. A. Ozin, *J. Mater. Chem*. **8**, *13,* 1998.

[56] X. Feng, G. E. Fryxell, L. Q. Wang, K. M. Kemner, *Science* **276**, *923*, 1997.

[57] L. Bronstein, E. Kramer, B. Berton, C. Burger, S. Forster, M. Antonietti, *Chem. Mater*. **11**, *1402*, 1999.

[58] Y. J. Han, J. M. Kim, G. D. Stucky, *Chem. Mater*.***12,*** *2068*, 2000.

[59] L. M. Bronstein, S. Polarz, B.Smarsly, M. Antonietti, *Adv. Mater*. **13,** *1333*, 2001.

[60] H. J. Shin, R. Ryoo, Z. Liu, O. Terasaki, *J. Am. Chem. Soc*. **123**, *1246,* 2001.

[61] X. Jiang, Y. Xie, J. Lu, L. Zhu, W. He, Y. Qian, *Chem. Mater*. **13**, *1213*, 2001.

[62] C. M. Yang, H. S. Sheu, K. J. Chao, *AdV. Funct. Mater*. **12**, *143*, 2002.

[63] H. Yang, A. Kuperman, N. Coombs, S. Mamiche, A. Ozin, *Nature* **379**, *705*, 1996.

[64] H. Yang, N. Coombs, G. A. Ozin, *Nature* **386**, *692*, 1997.

[65] J. R. Agger, M. W. Anderson, M. E. Pemble, O. Terasaki, Y. Nozue, *J. Phys. Chem. B* **102**, *3345*, 1998.

[66] V. I. Srdanov, I. Alxneit, G. D. Stucky, C. M. Reaves, S. M. DenBaars, *J. Phys. Chem. B* **102**, *3341*, 1998.

[67] H.Winkler, A. Birkner, V. Hagen, I. Wolf, R. Schmechel, H. von Seggern, R. A. Fisher, *Adv. Mater*. **11**, *1444*, 1999.

[68] H. Parala, H. Winkler, M. Kolbe, A. Wohlfart, R. A. Fischer, R. Schmechel, H. von Seggern, *Adv. Mater*. **12,** *1050*, 2000.

[69] S. Zheng, L. Gao, Q. H. Zhang, J.K Guo, *J.Mater.Chem.* **10**, *723*, 2000.

[70] M. Froba, R. Kohn, G. Bouffaud, *Chem. Mater*. **11**, *2858*, 1999.

[71] L.-Z. Wang, J.-L. Shi, W.-H. Zhang, M.-L. Ruan, J. Yu, D.S. Yan, *Chem. Mater.* **11,** *3015,* 1999.

[72] H. Kang, Y. W. Jun, J. L. Park, K. B. Lee, *Chem. Mater.* **12,** *3530*, 2000.

[73] R. Leon, D. Margolese, G. D. Stucky, *Phys. ReV. B* **52,** *2285, 1995*.

[74] F. Marlow, M. D. McGehee, D. Zhao, B. F. Chmelka, G. Stucky, *Adv. Mater*. **11,** *632*, 1999.

[75] P. Yang, et al. *Science* **287,** *465,* 2000.

[76] G. Wirnsberger, B. J. Scott,G.D.Stucky,*Chem.Comm.* **119**, 2001.

[77] G. Wirnsberger, B. J. Scott, B. F. Chmelka, G. D. Stucky, *Adv. Mater.* **12,** *1450*, 2000.

[78] C. J. Brinker, Y. Lu, A. Sellinger,H. Fan, *Adv. Mater*. **11**, *579,*1999.

[79] M. Trau, et al. *Nature* **390,** *674*, 1997.

[80] H. W. Hillhouse, T. Okubo, J. W. van Egmond, M. Tsapatsis, *Chem. Mater.* **9,** *1505*, 1997.

[81] N. A. Melosh, P. Davidson, P. Feng, D. J. Pine, B. F. Chmelka, *J.Am. Chem. Soc.* **123,** *1240*, 2001.

[82] S. H. Tolbert, A. Firouzi, G. D. Stucky, B. F. Chmelka, *Science,* **278,** *264,* 1997.

[83] H. Miyata, K. Kuroda, *J. Am. Chem. Soc*. **121**, *7618*, 1999.

[84] H. Miyata, K. Kuroda, *Adv. Mater.* **11,** *1448*, 1999.

[85] H. Miyata, K. Kuroda, *Chem. Mater.* **12,** *49*, 2000.

[86] H. Miyata, T. Noma, M. Watanabe, *Chem. Mater.* **14,** *766,* 2002.

[87] Ö. Çelik, Ö. Dağ, *Angew. Chem. Int. Ed*. **40**, *3800*, 2001.

[88] Ö. Dağ, O. Samarskaya, C. Tura, A. Gunay, Ö. Çelik, *Langmuir* **19,** *3671*,2003.

[89] Ö. Dağ, S. Alayoglu, C. Tura, Ö. Çelik, *Chem. Mater*. **15,** *2711*,2003.

[90] Ö. Dağ S. Alayoglu, I. Uysal, *J. Phys. Chem. B* **108**, *8439,* 2004.

[91] A.F. Dermirös, B.E. Eser, Ö. Dağ, *Langmuir* **21,** *4156*, 2005

[92] Ö. Dağ, A. Verma, C. T. Kresge, G.A. Ozin, *J. Mater. Chem*. **9**, *1475*, 1999.

[93] M. L, Steigerwald, L. E. Brus, *Acc. Chem. Res*. **23**, *183*, 1990.

[94] M. G. Bawendi, M. L. Steigerwald, L. Brus, *Annu. Rev. Phys. Che.* **41,** *477*, 1990.

[95] Y.Wang, N. Herron, *J. Phys. Chem*. **95,** *525,* 1991.

[96] H. Weller, *Adv. Mater*. **5**, *88*, 1993.

[97] A. P. Alivisatos, *Science* **271,** *933*, 1996.

[98] A.Eychmuller, *J. Phys. Chem. B* ***104,*** *6514,* 2000.

[99] M. G. Bawendi, W. L. Wilson, L. Rothberg, P. J. Carrol, T. M. Jedju, M. L.Steigerwald, L. E. Brus, *Phys. Rev. Lett*. **65**, *1623*, 1990.

[100] M. G. Bawendi, P. J. Carroll, W. Wilson, L.Brus, *J. Chem. Phys*. **96**, *1335,* 1992.

[101] W. Hoheisel, V. L. Volvin, C. S. Johnson, A. P. Alivisatos, *J. Chem. Phys*. **101,** *8455,* 1994.

[102] C. B. Murry, C. R. Kagan, M. G. Bawendi, *Science* **270**, *1335,* 1995.

[103] R. Rossetti, R. Hill, J. M.Gibson, L. E. Brus, *J. Chem. Phys*. **82**, *522*, 1995.

[104] H. Weller, *Angew. Chem. Int. Ed. Engl.* **32**, *41*, 1993.

[105] S. Mann, *Nature* **322,** *119*, 1988.

[106] C. B. Murray, D. J. Norris, M. G. Bawendi, *J. Am. Chem. Soc.* **115**, *8706*, 1993.

[107] N. C. Greenham, X. G. Peng, A. P. Alivisatos, *Phys. Rev. B* **54**, *17628,* 1996.

[108] V. L. Colvin, M. C. Schlamp, A. P.Alivisatos, *Nature* **370,** *354*, 1994.

[109] B. O. Dabbousi, M. G. Bawendi, O. Onitsuka, M. F. Rubner, *Appl. Phys. Lett.* **66**, *1316*, 1995.

[110] S. Gorer, J. A. Ganske, J. C. Hemminger, R. M. Penner, *J. Am. Chem. Soc.* **120**, *9584*, 1998.

[111] C. T. Tsai, D. S. Chuu, G. L. Chen, S. L. Yang, *J. Appl. Phys*. **79,** *9105,* 1996.

[112] J. Britt, C. Ferekides, *Appl. Phys. Lett*. **62**, *2851,*1993.

[113] B. J. Wu, H. Cheng, S. Guha, M. A. Haase, J. M. Depuydt, G. Meishaugen, J. Qiu, *Appl. Phys. Lett.* **63**, *2935,* 1993.

[114] S. Guha, B. J. Wu, H. Cheng and J. M. Depuydt, *Appl. Phys. Lett.* **63,** *2129,* 1993.

[115] Taguchi, T. Endoh, Y. Nozue, Y. *Appl. Phys. Lett*. **56**, *342,* 1991.

[116] T. Sugimoto, Monodispersed Particles, New York, 2001

[117] Z. A. Peng, X. Peng, *J. Am. Chem. Soc.* **124**, *3343,* 2002.

[118] C.Y. Cao, J. Wang, *J. Am. Chem. Soc.* **126,** *14337*,2004.

[119] R. B. Borade, *Zeolites* **7,** *398,*1987.

[120] R. Williams; P. N. Yocom, F. S. Stofko, *J. Colloid Interface Sc*i. **106,** *388*, 1985.

[121] Y. D. Li, H. W. Liao, Y. Ding, Y. Fan, Y. Zhang, Y. T. Qian, *Inorg. Chem*. **38,** *1382*, 1999.

[122] S. H. Yu, J. Yang, Z. H. Han, Y. Zhou, R. Y. Yang, Y. T. Qian, Y. Zhang, *J. Mater. Chem*. **9**, *1283*, 1999.

[123] N. Pradhan and S. Efrima, *J. Am. Chem. Soc*. **125**, *2050*,2003.

[124] S. M. Lee, Y. W. Jun, S. N. Cho, J. Cheon, *J. Am. Chem. Soc.* **122**, *11244*, 2002.

[125] X. Zhong, S. Liu, Z. Zhang, L. Li, Z. Wei, W. Knoll, *J. Mater. Chem.* **14**, *2790*, 2004.

[126] A. C. Jones, *Chem. Soc. Rev*. **101,** 1997.

[127] G. Henshaw, P. Parkin, G. Shaw, *Chem. Comm. 1095*, 1996.

[128] A. Heinglein, M. Gutierrez, Phys. Chem., 87, 852,1983. H. C. Youn, S. Baral, J. H. Fendler, *J. Phys. Chem.* **92**, *6320*,1988.

[129] T. Hirai, S. Shiojiri, I. Komasawa, *J. Chem. Eng. Jpn.* **27**, *590*,1994.

[130] B. Bhattacharjee, S. K. Mandal, K. Chakrabarti, D. Ganguli, S. Chaudhuri, J. *Phys. D: Appl. Phys*. **35**, *2636*, 2002.

[131] A K. Atta, P. K. Biswas, D. Ganguli, *Mater. Lett.* **15,** *99*,1992.

[132] G.K.Padam,G. L. Malhotra, S. U. M.Rao, *J. Appl. Phys.* **63**, *770*, 1988.

[133] Z. T. Zang, S. Dai, X. D. Fan, D. A. Blom, S. J. Pennycook, Y. Wei, *J. Phys. Chem. B* ***105,*** *6755*,2001.

[134] S. Wang, D. G. Choi, S. M. Yang, *Adv. Mater. **14,** 1311*, 2002.

[135] Z. Zhang, S. Dai, X. Fan, D. A. Blom, S. J. Pennycook, Y. Wei, *J. Phys. Chem. B* **105**, *29,* 2001.

[136] Ö. Dağ, I. Soten, Ö. Çelik, S. Polarz, N. Coombs, G. A.Ozin, *Adv. Funct. Mater*. ***13***, *30,* 2003.

[137] E. L. Crepaldi, D. Grosso, G. J. D. A. Soler-Illia, P. A. Albouny, H. Amenitsch, C. Sanchez, *Chem. Mater.* **14**, *3316*, 2002.

[138] L. E. Brus, *J. Chem. Phys.* **79**, *5566,* 1983

[139] S. Sapra, D. D. Sarma, *Phys. Rev. B* **69**, *125304,* 2004.

[140] S. Sapra, N. Shanthi, D. D. Sarma, *Phys. Rev. B* **66**, *205202*, 2002.

[141] A.F. Demirörs, Effect of Some Transition Metal Salts on The Synthesis of Mesoporous Silica, Ms Thesis, Bilkent University, 2005.